Singh. Arch Addict Rehabil 2017, 1(2):83-103
DOI: 10.36959/843/425 | Volume 1 | Issue 2

Review Article Open Access

Therapeutic Effects of Plant-Extract Synthesized Gold Nanoparticles against Alcohol-Induced Inflammatory Activity - A Proof of Concept

Singh AK*

Department of Veterinary Population Medicine, College of Veterinary Medicine, University of Minnesota, USA

Abstract

The present study describes potential beneficial and adverse effects of plant-extract synthesized gold nanoparticles (AuNPs) on ethanol toxicity in SH-SY5Y cells. Although Kudzu root extract (K), edible-gum extract (G), alone or in combination (KG), reduced Au^{3+} into AuNPs, the extract's composition and the reaction temperature determined their size ($AuNP_{KG\ (90 < 50 < 37)}$ << $AuNP_{K\ (90, 50 < 37)}$ < $AuNP_{G\ (90 < 50)}$; the subscript KG, K or G is extract identification and numerical are reaction temperature in Celsius) and biological properties ($AuNP_{KG\ (90, 50 > 37)}$ << $AuNP_{K\ (90, 50 > 37)}$ < $AuNP_{G\ (90, 50)}$). The surface of each AuNP contained the extract's active ingredients that were analyzed and confirmed using LDI and low-matrix MALDI. $AuNP_{KG\text{-}50}$ was (i) Least toxic to SH-SY5Y cells, but and most effective in suppressing the adverse effects of ethanol on SH-SY5Y cells and (ii) More effective than a combination of free kudzu and gum extracts. The beneficial and adverse effects of AuNPs may have been modified by the formation of proteins corona. This study provides a proof of concept for possible application of plant-extract synthesized AuNPs in mitigating alcoholism and ethanol toxicity.

Keywords

Ethanol, Gold nanoparticles, Plant extracts, Kudzu root, Edible gum, Cell viability, Apoptosis, Necrosis, Lactate dehydrogenase, Lipid peroxidase

Introduction

Alcoholism, a complex illness of the Central Nervous System (CNS), impacts the lives of millions around the world. Untreated alcoholism devastates families, depresses economic vitality, and burdens the country's health care systems, costing the U.S. over $249 billion annually [1-4]. Although possible mechanisms underlying the etiology of alcoholism are not fully understood, a critical role of opiate, Gamma Amino Butyric Acid (GABA), serotonin and NMDA/AMPA/Kainate receptors has been implicated [5-7]. Consequently, FDA has approved four drugs for treatment of alcoholism: naltrexone (an opiate antagonist), acamprosate (GABA receptors), disulfiram (acetaldehyde dehydrogenase inhibitor), and topiramate (AMPA/Kinate receptor), that can be used alone or in combination with psycho-behavioral therapies and counseling [8]. Many other receptor-based drugs are being developed for future use [9]. The current pharmacotherapy, although partially effective, has certain disadvantages. First, pharmacotherapy is a one-size-fits-all approach of addiction treatment that has not been largely successful, possibly because alcoholics constitute varying subtypes with differing biological and psychosocial contributions to the disease [10]. Second, alcoholism is a multifaceted disorder associated with neuro chemical heterogeneity and behavioral complexities, but current and prospective anti-alcoholism drugs selectively target specific receptors or transporters [8,9]. Therefore, patients may have to take many pills daily for comprehensive treatment/protection of alcoholism. This may be partially responsible for the patients' non-adherence to pharmacotherapy regimens. Third, the current

***Corresponding author:** Singh AK, Department of Veterinary Population Medicine, College of Veterinary Medicine, University of Minnesota, Twin-Cities Campus, St. Paul, MN 55108, USA, Tel: 763-234-9655, E-mail: singh001@umn.edu

Received: May 03, 2017; **Accepted:** August 10, 2017;

Published online: August 13, 2017

Citation: Singh AK (2017) Therapeutic Effects of Plant-Extract Synthesized Gold Nanoparticles against Alcohol-Induced Inflammatory Activity - A Proof of Concept. Arch Addict Rehabil 1(2):83-103

therapeutic drugs exhibit poor bioavailability, serious side effects and probability of development of addiction (for benzodiazepines).

Currently, the following alternative treatment approaches may constitute novel broad-spectrum pharmacotherapies for alcoholism and addiction.

- **Herbal medications:** Although many Asian countries have used medicinal plants such as *Tabernanthe iboga, Panax ginseng, Salvia miltiorrhiza, Hypericum perforatum, Pelargonium graveolens*, *Lippia citriodora*, *Punica granatum*, *Morinda citrifolia L, Mirabilis jalapa*, *Aloysia triphylla etc.* to treat addiction for centuries, only recently has the West begun to understand their pharmacological possibilities and clinical applications in alcoholism treatment [9-11]. Despite large volume of supporting research data, the clinical application of medicinal plants are hindered by their poor solubility and bioavailabity of the active ingredients, inability to cross the blood-brain barrier, and high variability [12].
- **Traditionally synthesized nanoparticles:** Development of Nanoparticle (NP)-based pharmacotherapy is a promising advancement in diagnosing and designing personalized treatment of addiction and other diseases. Studies have used colloidal gold and silver NPs, functionalized with multiple pharmaceuticals and other active ligands such as a blood-brain barrier permeant peptide, in treatment of alcoholism [13-15]. NPs, because of their unique properties, may circumvent the disadvantages of current pharmacotherapy by improving bioavailability and therapeutic efficacy of the drugs, loading multiple drugs in a single nanocarriers, improving compliance because patients will not have to take multiple pills, and facilitating on-demand drug release via external (UV or NIR beam or ultrasound) or internal (pH or selected enzymes) cues [16,17]. However, the traditionally synthesized gold and silver NPs have some disadvantages: they require stabilization to prevent rapid aggregation, difficult to functionalize with certain ligands, and undergo defunctionalization, releasing toxic NPs. Since the NPs contain the FDA approved drugs listed above, thus exhibit the same limitations listed above for pharmaceutical preparation.
- **Plant-extract synthesized nanoparticles:** Earlier studies have described synthesis of metal NPs using plant extracts (also known as 'green' synthesis) that are environment friendly, cost effective, easily scaled up for large scale syntheses, and do not require stabilizers such as polyethylene glycols [18-32]. Most importantly, the 'green' NPs retain the therapeutic potency of the plant and the unique properties of NPs. However, the key problems associated with the 'green' NPs are lack of methodology to identify the surface ligands, poor dose-response studies and lack of information regarding therapeutic doses.

Based on the observations discussed above, it is hypothesized that AuNPs synthesized with plant-extracts, especially using a combinations of kudzu root and gum extract because of their relevance to alcohol disorders [33-35], provides an effective and safe therapy for alcoholism and addiction. However, for broader acceptance, there is an urgent need to develop remedies for the disadvantages associated with plant-extract synthesized NPs. The overall goal of this study was to synthesize and characterize Gold Nanoparticles (AuNPs) using aquatic extract of kudzu root with or without edible gum. The specific aims were to (1) Characterize the AuNPs; (2) Identify and quantify the surface ligands; (3) Determine the AuNPs uptake into the SH-SY5Y cells and AuMP-protein interactions; (4) Assess the beneficial and adverse effects of AuNPs in SH-SY5Y cells. The methodologies were improved by including (i) An internal standard (4d-daidzein) in the extract used for synthesis of AuNPs preparations that allowed extract standardization and (ii) LDI and low-matrix MALDI for analysis of AuNP surface ligands. The preliminary studies indicated that inclusion of 'gum' in the reaction medium improved the AuNP's synthesis by kudzu root extract.

Materials and Methods

Preparation of plant extracts

Commercial, pre-calibrated, kudzu root extract powder (20 g, Sigma Chemicals) and 10 g Gum Arabic (Sigma Chemicals) were mixed in 100 ml Double Distilled Water (DDW) and incubated under stirring 50 °C for 4 h. The mixture was filtered through a 0.45 µm filter (Millex® poly vinylidene difluoride; EMD Millipore). The composition of the filtrate was analyzed as described in the supplementary section. The filtrate was freeze dried and stored at -80 °C for later use.

Nanoparticle synthesis and characterization

The traditional synthesis of AuNP using a reducing agent was performed as described by Singh, et al. [15]. For AuNP synthesis using plant extract, in a 250 ml flask, 1 mM $AuCl_3$ was mixed with 50 mL of filtered extracts (kudzu, gum, or mixture of the two) and 0.1 ml (1 mg/ml stock) of the internal standard (4d-daidzein) and heated to 37 °C, 50 °C and 90 °C that was maintained for 4 h (concentrations, temperature and time was determined in a preliminary study). The UV-Vis spectrum was measured at exaction band ranging from 500 to 600 nm to assess NP formation. After incubation (the preliminary study showed that 4 h of incubation at 50 °C or 2.5 h at 90 °C was sufficient for conversion of $AuCl_3$ to AuNPs,

5 to 10 nm), the mixture was centrifuged and the AuNP pellets were collected and washed 3 × with distilled water. Nanoparticles were characterized by measuring the following indices:

UV-VIS spectrum: Synthesized AuNPs were confirmed by sampling the aqueous component of different time intervals and the absorption maxima was scanned by UV-VIS spectrophotometer at the wavelength of 300-800 nm on Perkin-Elmer Lambda 25 spectrophotometer.

FT-IR spectrum: AuNP samples were dried and grinded with KBr pellets for FTIR measurements. The spectrum was recorded in the range of 4000-400 cm^{-1} using Varian FTS 1000 FT-IR Spectrometer in the diffuse reflectance mode operating at resolution of 4 cm^{-1}.

Surface topology by TEM: Morphology and size of the silver nanoparticles were investigated by TEM images using Hitachi model HF-2000 field emission transmission electron microscope with a resolution of 0.1 nm. Thin film of the sample was prepared on a carbon coated copper grid by just dropping a very small amount of the sample on the grid and drying under lamp.

Identification of AuNPs and the surface functional groups: Laser Desorption Ionization (LDI) without matrix and low-matrix-assisted LDI-TOF-MS (Bruker Autoflex III Smartbeam mass spectrometer that is equipped with a 355 nm Nd: YAG laser) were used to characterization of AuNP and functionalized groups. The nanoparticle preparations (1 µl) were mixed with 1 µL of (i) 50% acetonitrile (without matrix) and 0.1% Tri Floroacetic Acid (TFA) and (ii) 3 mg (for low-matric) and 20 mg (for full matrix) of α-Cyano-4-Hydroxy Cinnamic Acid (CHCA) solution. The mixtures were crystallized onto the LDI-disc. MS experiments were done in positive mode on a reflectron-type (20.92 kV) time-of-flight (to acquire a single spectrum, 200 laser shots were fired at a frequency of 100 Hz at 35-40% of the full laser power). In all cases, multiple spectra were averaged to obtain the reported data.

Beneficial efficacy and adverse effects of AuNPs

Beneficial and adverse effects of the AuNPs were investigated using SH SY5Y neuronal cell-lines. For culture, the vials containing SH SY5Y cells were thawed rapidly in a 37 °C water bath and the contents were transferred in a centrifuged tube containing 9.0 ml complete culture medium (1:1 mixture of Eagle's Minimum Essential Medium and F12 Medium mixed with fetal bovine serum, final concentration 10%). The cells were centrifuged at 125 × g for 7 minutes and the pellets were suspended with the complete medium (pH 7.0 to 7.6). The cells where incubated at 37 °C in 5% CO_2 in air atmosphere for 3 days. Then the cells were plated at a density of 10^7 cells in Cyto One filter cap flasks and cultured for 3 days. Then, the media was replaced with the one containing either different concentrations of AuNP preparations (AuNP-positive cells) or the matric alone

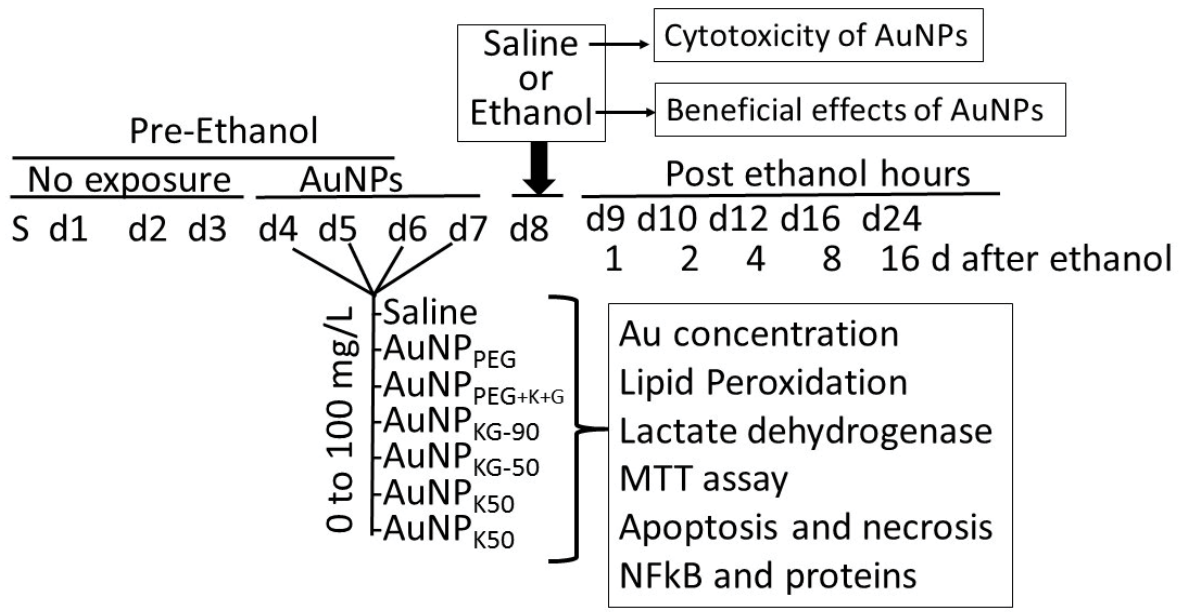

Figure 1: Experimental protocol. SH-SY5Y cells were expanded in growth media for 3 days. On day-4, 3 × 10^7 cells were transferred into each well and incubated for 4 days in media containing different doses of AuNPs (AuNP positive (A^p) cells) or matrix alone (AuNP negative (A^n) cells). At day-8, cells were washed and incubated in media containing 54 mM (final concentration) ethanol (A^p ethanol exposed (A^p/E^p) or An ethanol exposed (A^n/E^p) cells) or the matrix alone (AuNP and ethanol negative (A^n/E^n) or A^p ethanol negative (A^p/E^n) cells) for 24 hours. Then cells were washed and incubated in media alone. At different time intervals after ethanol exposure, cells were harvested and analyzed for AuNP internalization, AuNPs' adverse effects and modulation of ethanol toxicity.

(AuNP-negative cells) that continued for 4 days (day-4 to day-7). On day-8, cells were exposed for 24 h to either 50 mM ethanol (ethanol-positive cells) or saline (ethanol-negative cells) as matrix (Figure 1). This yielded the following cell groups: (1) AuNP-negative/ethanol-negative (A^n/E^n); (2) AuNP-negative/ethanol-positive (A^n/E^p); (3) AuNP-positive/ethanol-negative (A^p/E^n) and (4) AuNP-positive/ethanol-positive (A^p/E^p) cells (Figure 1). At day-9, the cells were incubated in AuNP and ethanol free culture media for another 16 days. At predetermined times (day-9 to day-25 (i.e. day-0 days post ethanol), cells were harvested and processed for the following:

Determination of internalized AuNPs by measuring intracellular Au concentrations (iAuCs): The Atomic Absorption Spectrometric method described by Pedersen and Graabaek [36] and Benlhabib, et al. [33,34] was used for analysis of Au in tissue samples. In brief, the cells were harvested, treated with trypsin, etched with Potassium Iodide (KI) and Iodine (I_2) at 1:6 ratio (0.34 mM I_2) to remove the surface AuNPs [37], washed with plasma buffered saline and mixed with 5 mL of aqua regia and digested for 24 h. The digest was diluted 1:1 with a solution of 2 ppm yttrium in dilute nitric acid serving as an internal standard. The instrument was calibrated using a solution of 1 ppm Au and 1 ppm yttrium in 50% aqua regia. The samples were introduced in a segment flow mode of a flameless atomic absorption spectrophotometer (Beckman model 485). Au concentration was determined using a calibration curve. The brain Au concentrations were normalized to total tissue weight.

Lactate dehydrogenase release assay: A 50 µl of clear cell media was mixed with the reconstituted 2 × LDH assay buffer (223 mg 2-p-iodophenyl-3-p-nitrophenyl-5-phenyl tetrazolium chloride, 57 mg N-methylphenazonium methyl sulfate, 575 mg NAD, and 3.2 g lactic acid in 480 ml 200 mM Tris buffer solution, pH 8.0). The mixture was gently shaken for 30 seconds and incubated in dark for 10 to 30 min at room temperature. Reaction was stopped woth 50 µl of Stop Solution (1M acetic acid), mixed and absorbance was measured between 490-520 nm [38].

Lipid peroxidase: The cells (3.6×10^6) were suspended in 2 ml of a solution containing 15% trichloroacetic acid, 0.25 N HCl and 0.5% thiobarbituric acid, and the samples were heated for 25 minutes in a boiling water bath. The samples were cooled and centrifuged for 10 min at 4,000 rpm. The absorbance of the supernatant fraction was determined at a wavelength of 535 nm. An extinction coefficient of 1.56×10^5 $M^{-1}cm^{-1}$ was used to calculate the concentration of malondialdehyde. Values were expressed as p mol of MDA per mg protein.

Cell viability: The MTT (3-(4,5-dimethylthiazol-2-yl)-2,5-diphenyltetrazolium bromide) tetrazolium reduction assay kit from Millipore (Chemicon, CT02) was used to assess cell viability.

Analysis of cells undergoing apoptosis and necrosis: Cells were exposed to the AuNPs followed by ethanol as shown in Figure 1. At different time intervals after cessation ethanol, the cells were harvested and double stained with Annexin V-FITC (An) and Propidium Iodide (PI) as described previously [15,38] and were subjected to FACS analysis using on a FAC Scan flow cytometer (Becton Dickinson, San Jose, CA). All the experiments were performed in triplicate. Cells were classified as An^-PI^- or An^+ PI^- (normal cells), An^-PI^{+++} (necrotic cells), $An^{++}PI^-$ (early apoptosis stage), $An^{+++}PI^+$ (late apoptosis stage).

NFkB activation by Electrophoretic Mobility Shift Assay (EMSA): Cell cultures from *in vitro* studies or finely chopped tissue samples from *in vivo* studies were suspended in HEPES hypotonic buffer A (10 mM HEPES, pH 7.9, 10 mM KCl, 0.1 mM EDTA, 0.1 mM EGTA, 1 mM Dm, 0.5 mM phenylmethylsulfonyl fluoride, and 10 pg/ml leupeptin, antipain, aprotinin, and pepstatin) for 15 min on ice. Samples were vortexed for 10 s with 0.6% Nonidet P-40 and centrifuged at 12,000 × g for 60 s. The pellets containing Nuclei were resuspended in nucleus buffer (20 mM HEPES, pH 7.9, 25% glycerol, 0.4 M NaCl, 1 mM EDTA, 1 mM EGTA, 1 mM DTT, 0.5 mM phenylmethylsulfonyl fluoride, and 10 pg/ml leupeptin, antipain, aprotinin, and pepstatin) and briefly sonicated on ice. For EMSA nuclear extracts (10 pg of protein) were incubated in 25 µl of total reaction volume containing 20 mM HEPES, pH 7.9, 50 mM NaCl, 0.1 mM EDTA, 1 mM DTT, 5% glycerol, 200 pg/ml bovine serum albumin, and 2.5 pg of poly(d1-dC) for 15 min at 4 °C. The Carboxytetramethyl-Rhodamine (TMR)-labeled oligonucleotide (0.5 ng) was then added to the reaction mixture and incubated for 20 min at room temperature [39].

RelA-p50 probe: TMR-AGT TGA GGG GAC TTT CCC AGG CAA-3

Reference probe: TMR-TCA ACT CCC CTG AAA GGG TCC GTT-5

Gels were scanned on the Hitachi FMBIO II using 585 channels for the isotope probe.

Characterization of AuNP-Protein Interaction

To investigate the AuNP-protein interaction, different AuNP preparations were incubated with fresh serum (1:10 by volume) at 37 °C for different time intervals. Thereafter, an equal volume of sucrose solution (0.75 M) was carefully layered and the samples were centrifuged at 10,000 g for 1 hour to separate unbound proteins (remained in water phase) from the AuNPs (settled at the bottom). The pellets were collected and washed three times with isotonic saline to remove soft corona. The

hard corona proteins were desorbed using CHAPS buffer (DNase 1 (100 U/mL), RNAse A (10 U/mL), $CaCl_2$ (20 mM), $MgCl_2$ (50 mM), Tris HCl pH 7 (100 mM), SDS 0.02%, ampholine (1%), CHAPS (0.8%), β-mercaptoethanol (1%) and urea (8 mM)). The mixture was centrifuged (15,000 rpm, 3 min) to separate the AuNPs (in the pellets) and the desorbed proteins (in the supernatant). The desorbed proteins were concentrated, mixed with Bromophenol blue (0.5 µL) and run on 1-DE gels. The separated proteins were staining with Coomassie dye or viewed for fluorescence under UV light [40].

For protein identification, the surface-adsorbed proteins were reduced with 10 mM Dithiotreitol (DTT) at 37 °C for 1 h and alkylated with 25 mM Iodoacetamide (IAA) at room temperature for 50 min. For the digestion, the samples were incubated with porcine trypsin (Promega) for 8 h at 37 °C. The digested peptides were concentrated and purified in reverse phase C18 µcolumn and eluted with the acid solution consisting of 10 mg/mL in 50% acetonitrile/Milli-Q water (v/v), 0.1% Tri Fluoraceticacid (TFA)).

An Agilent-1100 nano flow LC system (equipped with a solvent degasser, nano-flow pump and, temperature controlled auto sampler, a 7 Tesla Finnegan Linear Quadrupole Ion Trap Fourier Transform (LTQ-FT) mass spectrometer and an LTQ-Orbitrap from Thermo Electron, Bremen, Germany) was used for nanoscale liquid chromatography tandem mass spectrometry of the digested peptides. Tryptic peptides were separated on 30 cm reverse phase columns (75 µm inner diameter (SGE analytical) mounted on the nano-electro spray ion source at a flow rate of 250 ml/min and were separated over 30 min using a linear gradient of 10-40 (v/v) acetonitrile/0.5% (v/v) acetic acid). For MS, the applied voltage was 2.4 kV to the emitter. Full scan MS spectra (from m/z 300-1,575) were acquired in the ICR with a resolution R = 25,000 at m/z 400 (after accumulation to a target value of 5×10^6 in the linear ion trap). The ions monitored are listed in Table 1.

For immune staining, the separated proteins were transferred onto a PVDF membrane, blocked and incubated with rabbit anti-mammalian-IgG selective antibodies (reactivity to rat proteins were predetermined), followed by Horse Radish Peroxidase (HRP)-conjugated goat anti-rabbit IgG antibodies. For detection, an HRP-conjugated secondary antibody enhanced chemiluminescence kits from Abcam were used.

Statistical analysis

Data were recorded as mean ± SD using Microsoft Excel. Statistical analysis was performed using ANOVA followed by Tukey's Multiple-Comparison Test or t-test at < 0.05 significance level.

Results

Nanoparticle synthesis and characterization

Physicochemical characterization: $AuCl_4^-$ (a yellow colored aqueous solution) exhibited strong absorption at 217 nm and a weak absorption at 287 nm. Exposure of $AuCl_4^-$ to reducing agents immediately changed its color from yellow to red/brown characterized by a strong absorption from 500-665 nm range, depending upon the nanoparticle size and synthesis procedure (Figure 2a). A combination of Kudzu and Gum (KG) extract at 90 °C, 50 °C and 37 °C yielded AuNPs with average diameter of 8 nm, 12 nm and 20 nm, respectively (Figure 2b). The Kudzu (K) extract alone at 90 °C, 50 °C and 37 °C formed relatively larger AuNPs (diameter 30 to > 50 nm). The Gum solution (G) alone yielded particle > 50 nm in diameter. The FTIR spectra of K extract and different nanoparticles are shown in Figure 3. The extract exhibited strong absorption at 2928, 1641, 1382 and 1069 cm^{-1}, and weak absorption at 1456, 1156 and < 500 cm^{-1}. The AuNPs (i: $AuNP_{KG-50}$; ii: $AuNP_{KG-95}$ and iii: $AuNP_K$) exhibited strong absorption at 3420, 1609 and1078 1069 cm^{-1}, and weak absorption at 2920, 1456, 1383, 1156, 981 and < 500 cm^{-1}) (Figure 2 and Figure 3).

The surface characterization: Low-matrix MALDI detected Au^+ (m/z 193), Au^{2+} (m/z 396) and Au^{3+} (m/z

Table 1: List of fragment ions monitored for protein identification.

Protein	Test: IS or MS: sequence	m/z (+1)	m/z (+2)
Bin1 protein	MS: AEEELIK	832.2	418.1
Casein Kinase 1 γ2	MS: MEYVHTK	908.0	456.3
cAMP/cGMP phosphodiesterase	MS: VOYHNWK	944.4	-
Glutaryl-Co-A dehydrogenase	MS: CEDNCIR	853.3	439.1
Arginine N-methyltransferase	MS: QYKDYK	845.5	424.3
Lactate dehydrogenase	MS: MVSGESR	766.52	384.3
MAPK kinase 7	MS: LCDFGISGR	968.7	-
Parvalbumin	MS: FFQMVGLK	970.5	486.4
Protein Tyr Phosphatase	MS: MPVIVSR	803.1	-
Transferrin	MS: EDPQTFYY	815.5	209.3
Triose phosphate isomerase	MS: AISDNVK	731.4	-

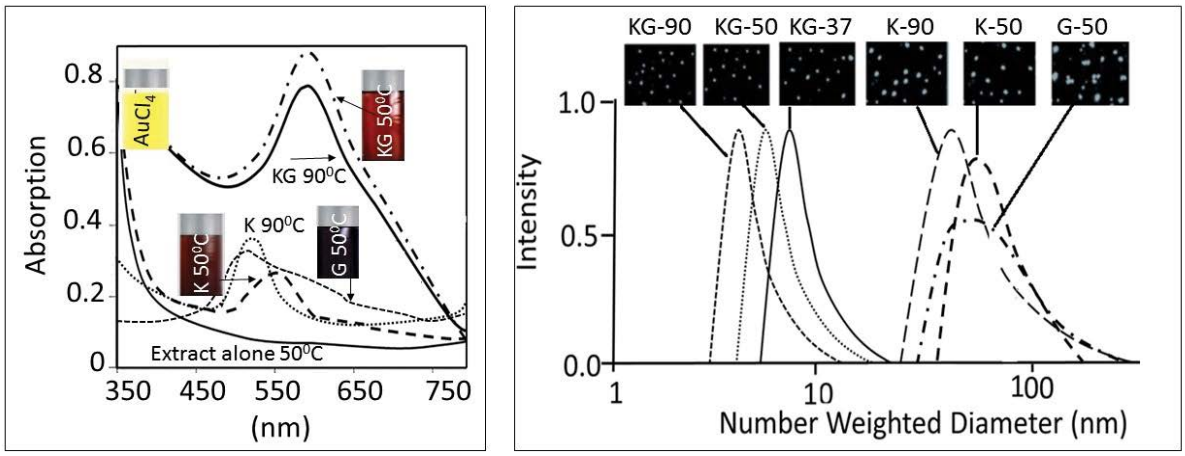

Figure 2: Typical FTIR spectra for $AuNP_{KG}$, kudzu extracts and gum solution.

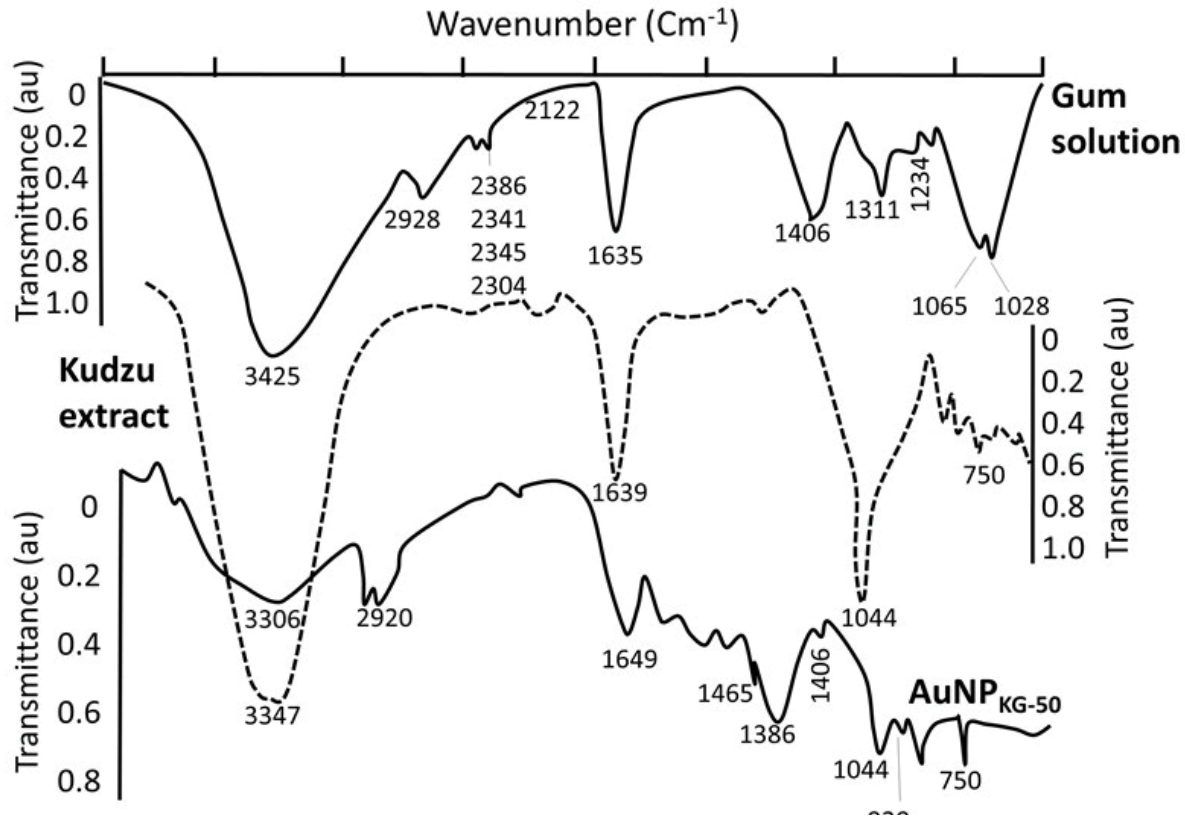

Figure 3: Optical absorption curves (A), size distribution (B) and transmission electron microscopy of different AuNP preparations.

Abbreviations: K: Kudzu; G: Gum; 37, 50 and 90: Reaction temperature in °C.

589) (Figure 4A). The LDI-TOF MS detached the surface ligands for $AuNP_{KG}$ (Figure 4B), free standards (Figure 4C), $AuNP_G$ (Figure 4D), $AuNP_K$ (Figure 4E) and blank (Figure 4F). The identity of fragment ions was confirmed by analyzing components of kudzu root extract (daidzein, d4-daidzein internal standard, puerarin, and kakkasapon in III) and gum solution (arabinose, galactose, and fructose). This suggests that, when nanoparticles are synthesized with plant extract, their components adsorb onto the surface (Figure 4).

AuNPs internalization in cells

The dose-internalization curves for different AuNPs (measured as iAuC) were linear from 5 to 100 mg/L AuNP dose (Figure 5). The r^2 for A^P/E^n and A^P/E^P cells ranged from 0.97 to 0.99 and 0.78 to 0.95, respectively, indicating greater variability in A^P/E^P cells. As shown below, the iAuCs were highest in cells exposed to AuN-

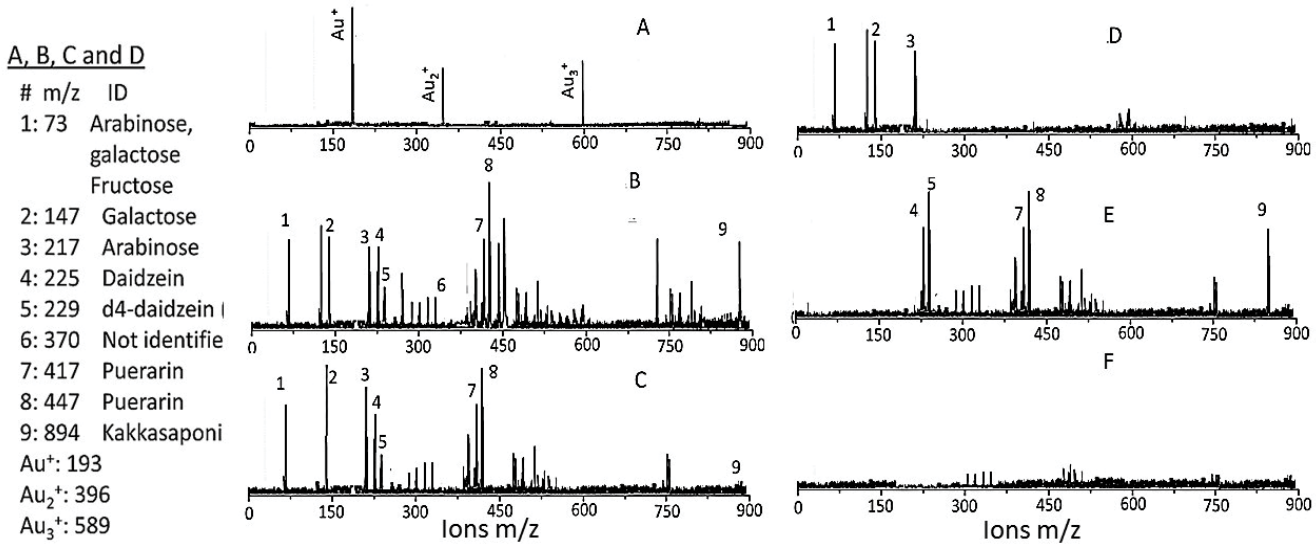

Figure 4: Mass spectral identification of surface ligands. A: Low-level matrix-LDI that detects Au ions; B: Typical LDI (matric free) analysis of $AuNP_{KG-50}$ synthesized by a mixture of kudzu root and gum; C: Typical LDI analysis of a mixture of kudzu and gum solutions; D: Typical LDI (matric free) analysis of $AuNP_{G-50}$ synthesized by a gum solution alone; E: Typical LDI (matric free) analysis of $AuNP_{K-50}$ synthesized by a kudzu extract alone; and F: Analysis of a blank solution.

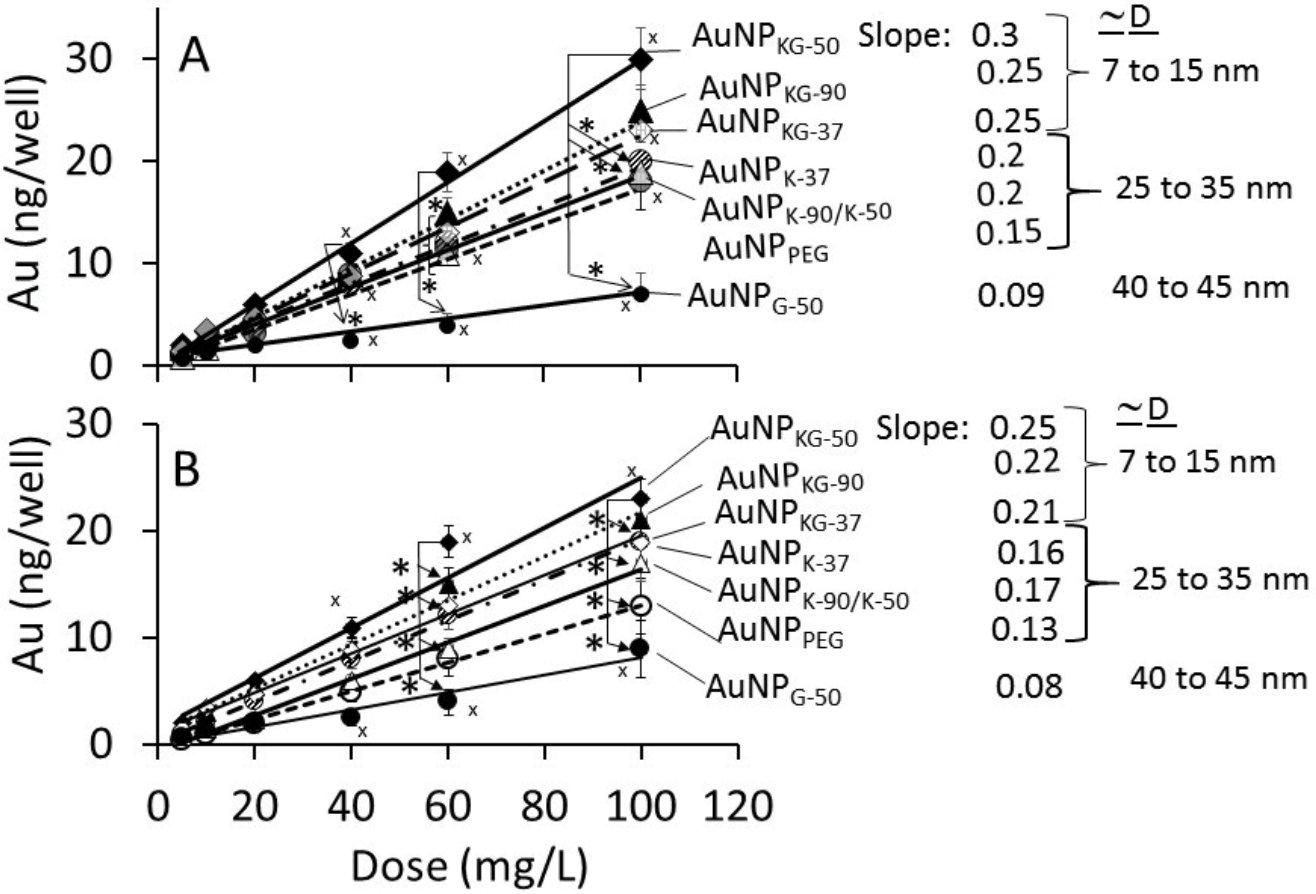

Figure 5: The dose (mg/L of AuNPs) versus response (intracellular Au concentration-iAuC) curves for internalization of different AuNPs at day-16 of cell incubation. A: A^p/E^n cells and B: A^p/E^p cells. Values are mean ± SD.

P_{KG-50} and lowest in cells exposed to $AuNP_G$. The slops of the curve ranged from 0.06 to 0.1 (Figure 5).

A^p/E^n cells: $AuNP_{KG-50} > AuNP_{KG - 90, KG-37, K-37} > AuNP_{K-37, k-50, k-90, PEG+K+G} > AuMP_{G-50}$

A^p/E^p cells: $AuNP_{KG-50}$ > $AuNP_{KG-90,\ KG-37,\ K-37}$ > $AuNP_{k-50,\ K-90}$ > $AuNP_{PEG+K+G}$ > $AuMP_{G-50}$

Figure 6 shows the time-course of iAuC changes in cells harvested at (i) Culture days 4 to 7 (days 1 to 4 of AuNP exposure), (ii) Culture day 8 (24 h ethanol exposure), and (iii) Culture day 9, 10, 14, 18 and 26 (16 days free of ethanol an NPs) as shown in Figure 1. From day-4 to day-7, iAuCs increased gradually and, at day-4, the iAuCs showed the following pattern: $AuNP_{KG-90,}$ $AuNP_{KG-50}$ and $AuNP_{KG-37}$ > $AuNP_{K-90,}$ $AuNP_{K-50}$ and $AuNP_{K-37}$ > $AuNP_{PEG}$ and $AuNP_{G-50}$. In A^p/E^n cells, a linear decrease in iAuCs occurred. The values at day-24 (16 days after discontinuation ethanol) ranged from 0 to 4 ng/well. In A^p/E^p cells, the post-ethanol iAuCs were significantly lower than those in corresponding A^p/E^n cells (Figure 6). The day-24 (16 days after discontinuation of ethanol) values for A^p/E^p and A^p/E^n cells did not differ significantly (Figure 6).

Characterization of surface ligands in AuNPs collected from exposed cells

Figure 7 shows a typical time-course of change in surface ligands of intracellular $AuNP_{KG-50}$ at different time intervals in A^p/E^n cells (Figure 7A - $fAuNP_1$, $fAuNP_2$, $fAuNP_4$, $fAuNP_8$, $fAuNP_{16}$ represent 1, 2, 4, 8 and 16 days after ethanol exposure). Figure 7B shows time-course of change in total number of peaks observed onto the $AuNP_{KG-50}$ surface. The peak numbers remained unchanged for up to 8 days, but decreased significantly at day-16 after ethanol exposure. The N^p/E^n values were significantly higher than the A^p/E^p values. This may be due to desorption and degradation of the ligands. Figure 7C shows a linear relationship between the $AuNP_{KG-50}$ dose and the IS-peak-area/ligand-peak-area ratio (Figure 7).

Beneficial and adverse effects of AuNPs

To evaluate the adverse effect of AuNPs alone, A^p/E^n cells were exposed to different concentrations of individual AuNPs for 4 days, the saline (matrix for ethanol) for 24 h. The cells were assayed for (i) Viability using MTT metabolism assay, (ii) Apoptotic and necrotic cells, and (iii) Lipid peroxidase and lactate dehydrogenase activities. The beneficial effects were studied by incubating A^p/E^p cells with different doses of AuNPs for 4 days, followed by 50 mM ethanol, and then assayed as above.

Cell viability:

Dose-response: In A^p/E^n cells, a 5, 10, 20, 40 or 60 mg/L dose of different AuNP preparations did not significantly affect, while a 100 mg/L dose of AuNPs caused

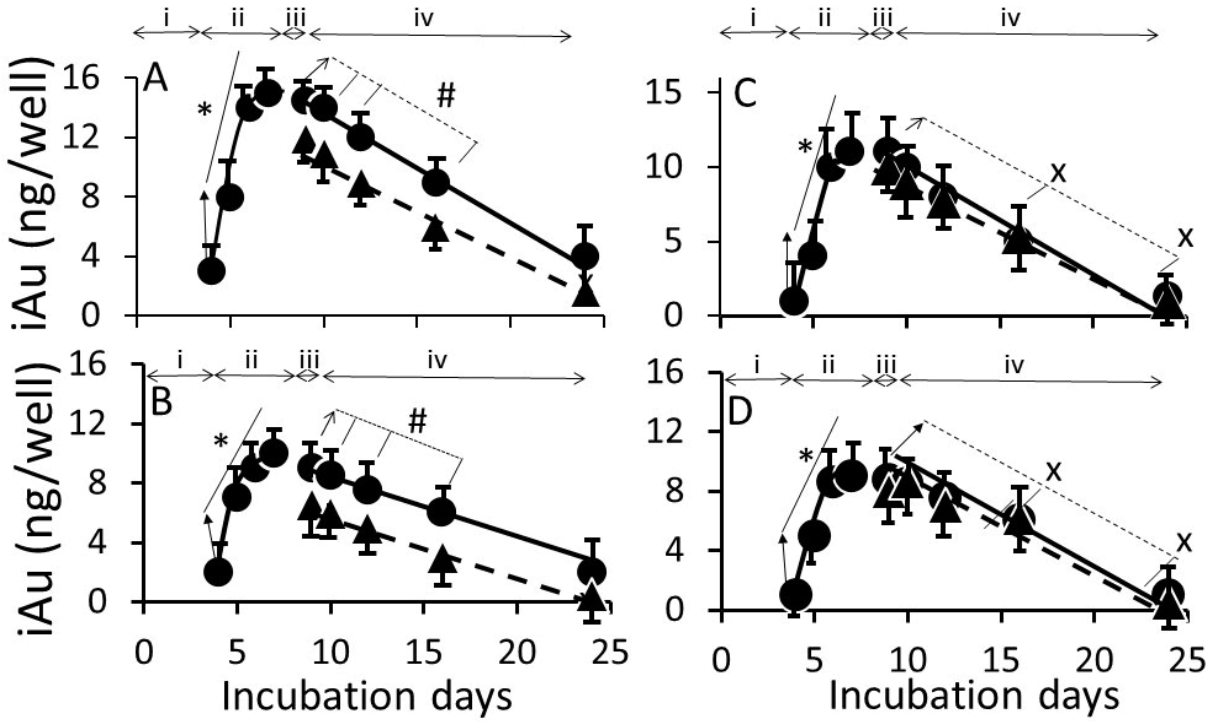

Figure 6: The time-course of change intracellular $AuNP_{KG-50}$ (A), $AuNP_{K-50}$ (B), $AuNP_{G-50}$ (C) and $AiNP_{PEG+K+G}$ concentrations in A^p/E^n cells (solid line) and B: A^p/E^p cells (broken line).

x: $p < 0.05$ when day-8 (before ethanol/matrix exposure) values were compared with post-ethanol values; #: $p < 0.05$ when corresponding A^p/E^n values were compared with corresponding A^n/E^p values.

Abbreviations: i: Three days of cell growth (days 1 to 3); ii: Four days of AuNP or matrix pretreatment (day-4 to day-7); iii: 24 h ethanol or saline (matrix) exposure (day-8); iv: AuNP and ethanol free media for 16 days.

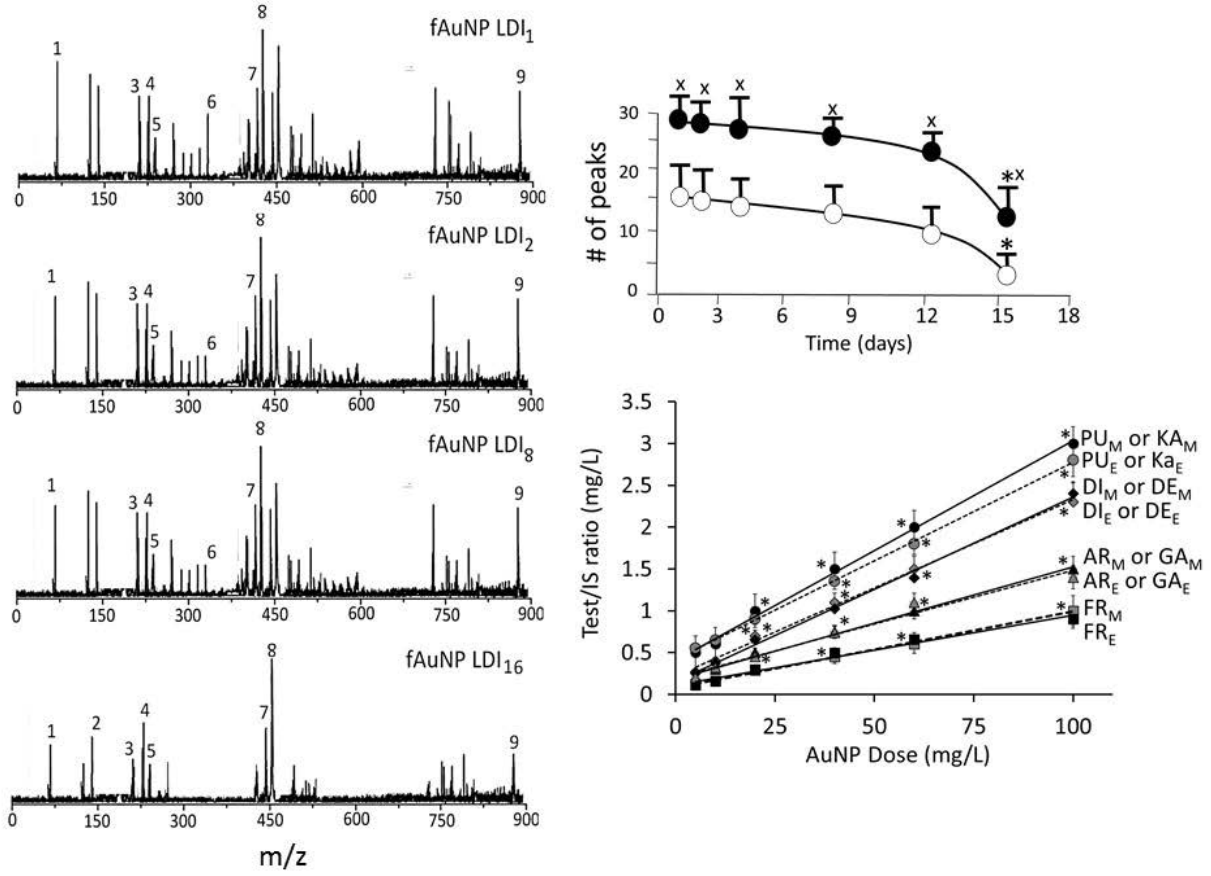

Figure 7: Identification of surface ligands on AuNPs collected from A^p/E^n and A^p/E^p cells. A: the plant component peaks at 1 ($fAuNP\ LDI_1$), 2 ($fAuNP\ LDI_2$), 4 ($fAuNP\ LDI_4$), 8 ($fAuNP\ LDI_8$) and 16 ($fAuNP\ LDI_{16}$) days after ethanol exposure; B: Time-course of change in total number of peaks adsorbed onto the AuNP surface. Total number of peaks decreased significantly at day-16.

The time-course of change in intracellular AuNPs as measured by iAuCs. A: Intracellular $AuNP_{KG-50}$; B: Intracellular $AuNP_{K-50}$; C: Intracellular $AuNP_{G-50}$; D: Intracellular $AuNP_{PEG}$ in A^p/E^n cells (filled circle) and A^p/E^p cells (open circle). C: AuNP dose versus (ligand peak/IS peak) ratio plots for (i) PU_M, KA_M, DI_M, DE_M, AR_M, GA_M, FR_M in $AuNP_{KG-50}$ isolated from A^p/E^n cells, and (ii) PU_E, KA_E, DI_E, DE_E, AR_E, GA_E, FR_E in $AuNP_{KG-50}$ isolated from A^p/E^p cells. A linear response between AuNP dose vs. ligand/IS ratio suggest that a dose-response could established by using the ligand concentration as the dose. Values are mean ± SD.

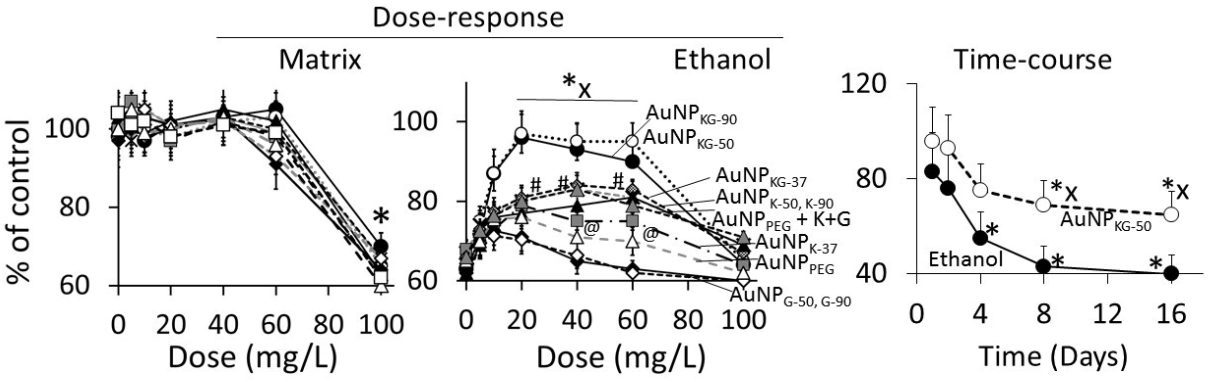

Figure 8: (A) Plots of dose (AuNP mg/L) *versus* viable A^p/E^n cells (% of control) at day-16). A 5 to 60 mg/L dose of all AuNP exhibited comparable response. Only 100 mg/L dose caused significant decrease in viable cell enumeration. Values are mean ± SD; (B) Plots of dose (AuNP mg/L) *versus* viable A^p/E^p cells (% of control) at day-16). Different AuNPs yielded variable response, but maximum protection was provided by $AuNP_{KG-50, -90}$ at 20 mg/L dose. Values are mean ± SD. *: $p < 0.05$ when compared with A^n/E^n response and x, # or @: $p < 0.05$, when viability of A^p/E^p cells exposed to a given dose of and AuNP compared with viability of A^p/E^p exposed to the same dose of other AuNPs; (C) The time-course of change in viability of A^p/E^n (broken line) and A^p/E^p (solid line) cell pre-exposed to a 20 mg/L dose of $AuNP_{KG-50}$. *: $p < 0.05$ when exposed to day-0 values and x: $p < 0.05$ when A^p/E^n and A^p/E^p values were compared at each time interval.

30% to 60% decrease in viable cells (Figure 8A, hour-16 data). Ethanol exposure of A^n/E^p and A^p/E^p cells significantly decreased cell viability (Figure 8B). A 5, 10, 20, 40 or 60 mg/L dose of different AuNP preparations protected (10% to 40% reduction in MTT response) against the ethanol-induced decrease in cell viability ($AuNP_{KG-50\ or\ KG-90}$ > $AuNP_{KG-37}$ > $AuNP_{K-90,\ K-50}$ > $AuNP_{K37}$, $AuNP_{PEG+K+G,}$ > $AuNP_{G-50\ or\ G90}$ or $AuNP_{PEG}$). A 100 mg/L dose of all AuNP preparations either did not change or augmented ethanol toxicity. This suggests that the 20 and 40 mg/L dose of $AuNP_{KG-50}$ and $AuNP_{KG-90}$ were most effective against ethanol toxicity in SH-SY5Y cells.

Time-course: At 1 and 2 days after cessation of ethanol exposure in $AuNP_{KG-50}$-pretreated (A^p/E^p) or $AuNP_{KG-50}$-negative (A^n/E^p) cells, about 70% of total cells were viable and the values did not differ significantly between the two cell groups. Thereafter, the $AuNP_{KG-50}$-pretreated values were significantly greater than $AuNP_{KG-50}$-ve cells at all time intervals (Figure 8).

Lipid peroxidase and lactate dehydrogenase activities:

Dose response: In A^p/E^n cells, a 5, 10, 20, or 40 mg/L dose of all AuNP preparations did not increase, a 60 mg/L dose slightly increased, and a 100 mg/L dose significantly increased the enzyme activities (Figure 9A for lipid peroxidase and Figure 10A for LDH). The enzyme activities (Figure 9A for lipid peroxidase and Figure 10A for LDH) showed the following patterns in A^p/E^n cells: $AuNP_{G-50}$ and $AuNP_{K-90}$ >> $AuNP_{PEG}$ > $AuNP_{PEG+K+G,}$ $AuNP_{KG-50,}$ $AuNP_{KG-37}$ and $AuNP_{KG-90}$. In A^n/E^p cells or A^p/E^p cells, exposure to $AuNP_{G-50}$, $AuNP_{K-90,}$ $AuNP_{K-50}$, $AuNP_{KG-37,}$ $AuNP_{PEG}$ and $AuNP_{PEG+K+G}$ caused 125% to 155% increase in the enzyme activities (Figure 9B for lipid peroxidase and Figure 10B for LDH). In A^p/E^p cells, exposure to $AuNP_{KG-50}$ or $AuNP_{KG-90}$ (dose: 20, 40 and 60 mg/L) ethanol exposure did not significantly increased the enzyme activities (Figure 9B for lipid peroxidase and Figure 10B for LDH). However, ethanol exposure of $AuNP_{KG-50}$ pretreated (dose: 100 mg/L) cells significantly increased the enzyme activities. This suggests that a 20 to 60 mg/L dose of $AuNP_{KG-50}$ or $AuNP_{KG-90}$ protected A^p/E^p cells against ethanol toxicity (Figure 9 and Figure 10).

Time-course (Figure 9C for lipid peroxidase and Figure 10C for LDH): The two enzymes exhibited different time-course of change in response to ethanol exposure. Lipid peroxidase activities were significantly higher at day-1 and day-2, and then decreased gradually to 130% of control at day-16. The ethanol-induced increase in peroxidase activity in A^n/E^p cells were significantly greater than the activity in A^p/E^p ($AuNP_{KG-37,\ -50\ -90}$ pretreated, 20 mg/L) cells, indicating neutralization of ethanol-induced oxidative stress by $AuNP_{KG}$. Other AuNPs were variably effective, providing < 20% protection. Unlike lipid peroxidase activities, LDH activities increased gradually and peaked at day-4. Then a gradual decrease occurred. LDH activities in A^n/E^p cells and A^p/E^p ($AuNP_{KG}$ pretreated) cells did not differ significantly

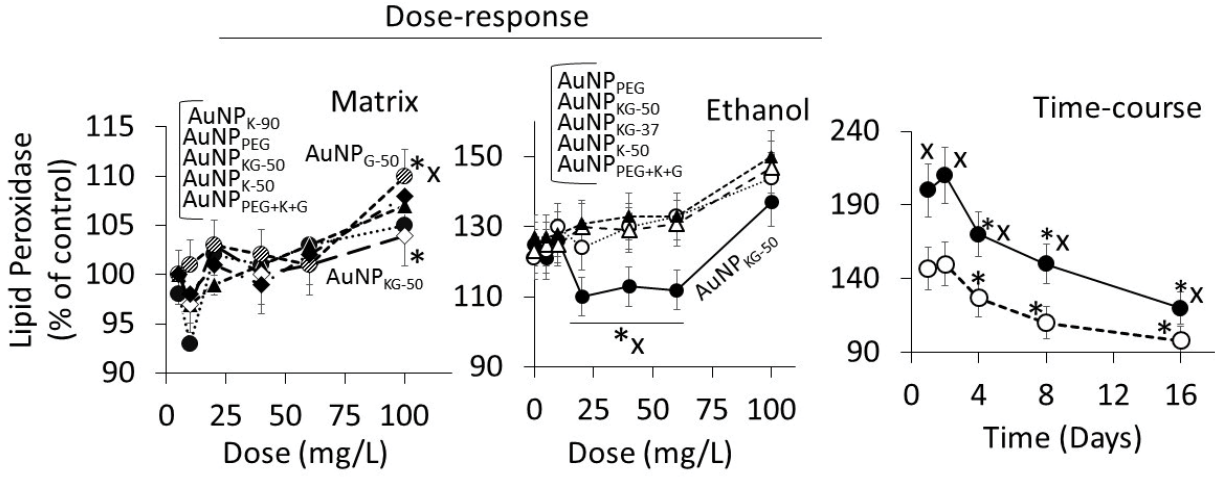

Figure 9: (A) Plots of dose (AuNP mg/L) *versus* intracellular lipid peroxidase activity in cells A^p/E^n (% of control) at day-16. A 5 to 60 mg/L dose of all AuNP exhibited comparable response. Only 100 mg/L dose caused significant but variable increase in enzyme activity ($AuNP_{KG-50}$ exhibited lowest, while $AuNP_{G-50}$ exhibited highest activity in response to 100 mg/L dose). Values are mean ± SD; (B) Plots of dose (AuNP mg/L) *versus* intracellular lipid peroxidase activity in A^p/E^p cells (% of control) at day-16. Different AuNPs yielded variable response, but maximum protection was provided by $AuNP_{KG-50}$ at 20 to 60 mg/L dose. Values are mean ± SD. *: $p<0.05$ when A^p/E^n or A^p/E^p values were compared with A^n/E^n values. X, # or @: $p < 0.05$, when enzyme activity of A^p/E^p cells exposed to a given dose of and AuNP compared with enzyme activity of A^p/E^p cells exposed to the same dose of other AuNPs; (C) The time-course of change in enzyme activity of A^p/E^n (broken line) and A^p/E^p (solid line) cell pre-exposed to a 20 mg/L dose of $AuNP_{KG-50}$. *: $p < 0.05$ when exposed to day-0 values and x: $p < 0.05$ when A^p/E^n and A^p/E^p values were compared at each time interval.

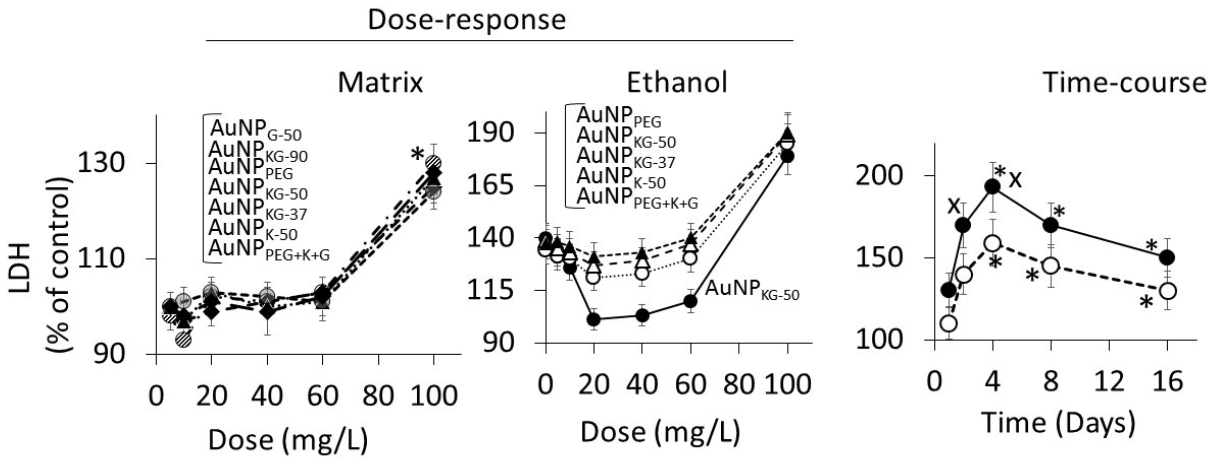

Figure 10: (A) Plots of dose (AuNP mg/L) *versus* Lactate Dehydrogenase (LDH) activity in A^p/E^n cells (% of control) at day-16. A 5 to 60 mg/L dose of all AuNP exhibited comparable response. Only 100 mg/L dose caused significant in enzyme activity. Values are mean ± SD; (B) Plots of dose (AuNP mg/L) *versus* LDH activity in A^p/E^p cells (% of control) at day-16. Maximum protection was provided by $AuNP_{KG-50}$ at 20 to 60 mg/L dose. Values are mean ± SD. *: $p < 0.05$ when A^p/E^n or A^p/E^p values were compared with A^n/E^n values, x: $p < 0.05$, when enzyme activity of A^p/E^p cells exposed to a given dose of and AuNP compared with enzyme activity of A^p/E^p cells exposed to the same dose of other AuNPs; (C) The time-course of change in LDH activity of A^p/E^n (broken line) and A^p/E^p (solid line) cells pre-exposed to a 20 mg/L dose of $AuNP_{KG-50}$. *: $p < 0.05$ when exposed to day-0 values and x: $p < 0.05$ when A^p/E^n and A^p/E^p values were compared at each time interval.

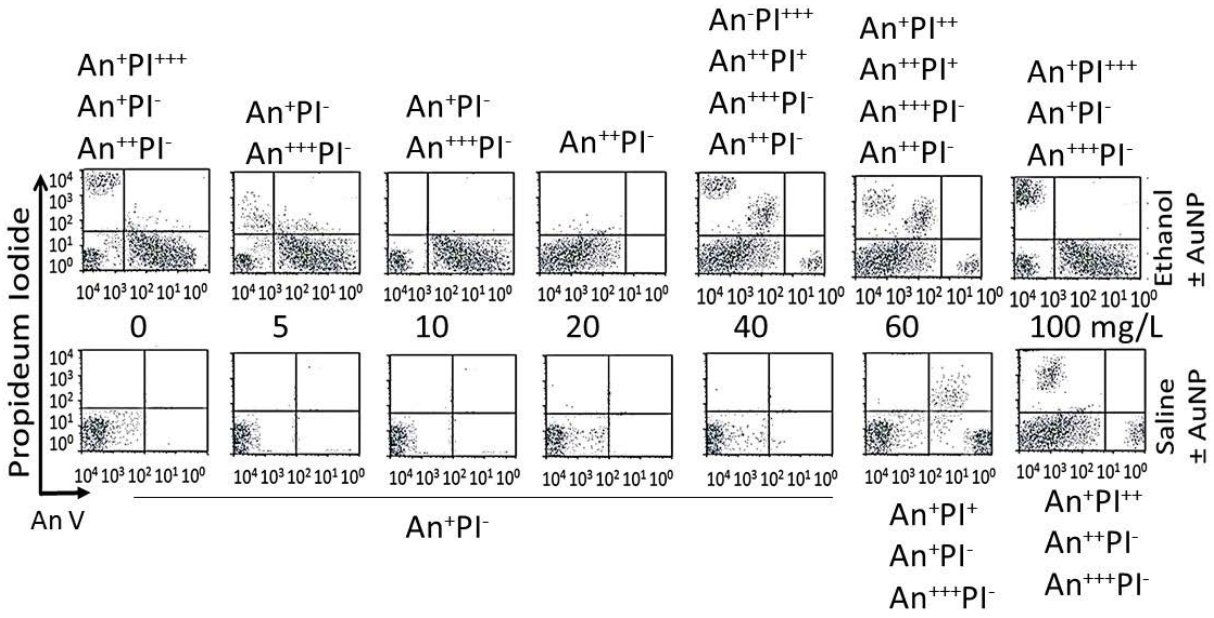

Figure 11: Effects of different doses of AuNPs on incorporation of annexin V and propidium iodide (PI) in A^n/E^n (bottom 0 mg/L), A^p/E^n (bottom 5 to 100 mg/L), A^p/E^p (top 5 to 100 mg/L AuNP) and A^n/E^p (top 0 mg/L) cells.

at days 1, 8 or 16, but differed significantly at days 2 and 4. Other AuNPs were variably effective, showing 5% to 30% increase (Figure 9 and Figure 10).

Enumeration of apoptotic and necrotic cells:

Dose-response (16-day data): Figure 11 shows distribution of different cell phenotypes in A^n/E^n, A^p/E^n (different AuNP dose) and A^p/E^p cells. A^n/E^n and A^p/E^n (5 to 40 mg/L AuNP dose) cells exhibited mostly An^-PI^- phenotypes. A^p/E^n (60 mg/L AuNP dose) cells exhibited An^-PI^- and $An^{+++}PI^-$ phenotypes, while A^p/E^n (100 mg/L AuNP dose) exhibited An^+PI^-, $An^{+++}PI^-$ and An^+PI^{++} phenotypes. This suggests that 5 to 40 mg/L doses of $AuNP_{KG-50}$ did not induced apoptosis or necrosis in cell cultured. The cell phenotypes in A^p/E^n cells exposed to other AuNPs are shown in Table 2.

A^n/E^p cells exhibited An^+PI^-, $An^{++}PI^-$ and An^+PI^{+++} phenotypes. The A^p/E^p ($AuNP_{KG}$ dose 5 and 10 mg/L) cells exhibited An^-PI^- and $An^{++}PI^-$ phenotypes. A^p/E^p

Table 2: Effects of AuNP dose on sh-sy5y cell phenotype.

NP (mg/L)	0	5	10	20	40	60	100
A^n/E^n cells (no AuNPs or ethanol)							
-	An^-PI^-	-	-	-	-	-	-
A^p/E^n cells (AuNPs positive but ethanol negative)							
$AuNP_{KG-90, 50, 37}$ $AuNP_{K-90, 50, 37}$	-	An^-PI^-	An^-PI^-	An^-PI^-	An^-PI^-	$An^{++}PI^-$	An^-PI^- $An^{++}PI^+$ $An^{+++}PI^+$
$AuNP_{G-50, 90}$	-	An^+PI^-	An^+PI^-	An^+PI^-	An^+PI^-	An^+PI^-	An^-PI^- $An^{+++}PI^-$ An^+PI^{++}
$AuNP_{PEG, PEG+K+G}$	-	An^+PI^-	An^+PI^-	$An^{l+}PI^-$	$An^{++}PI^-$	$An^{+++}PI^-$ $An^{++}PI^-$ An^+PI^+	An^+PI^- $An^{+++}PI^+$ An^-PI^{++}
A^n/E^p cells (AuNPs negative, but ethanol positive)							
	An^-PI^{+++} $An^{++}PI^-$ An^+PI^{++} $An^{+++}PI^-$	-	-	-	-	-	-
A^p/E^p cells (AuNPs and ethanol positive)							
$AuNP_{KG-90, -50, -37}$	-	An^-PI^- $An^{++}PI^-$ $An^{++}PI^+$	$An^{++}PI^-$	$An^{++}PI^-$	$An^{++}PI^-$	An^+PI^- An^+PI^+ $An^{++}PI^+$	An^-PI^- $An^{++}PI^+$ An^-PI^{++}
$AuNP_{K-90, -50, -37}$	-	An^-PI^- $An^{++}PI^-$ $An^{++}PI^+$	An^-PI^- An^+PI^+	An^+PI^- An^+PI^{++}	An^+PI^- An^+PI^{++}	An^-PI^- $An^{++}PI^+$	An^-PI^+ $An^{++}PI^-$ $An^{++}PI^{++}$
$AuNP_{G-50, -90}$	-	An^-PI^- An^+PI^{++}	An^+PI^- An^+PI^{++}	An^+PI^- An^+PI^+	An^+PI^- $An^{++}PI^+$ An^+PI^+	An^+PI^- $An^{++}PI^+$ An^-PI^+	An^-PI^+ $An^{++}PI^-$ $An^{++}PI^+$
$AuNP_{PEG, PEG+K+G}$	-	$An^{++}PI^-$	$An^{++}PI^-$ $An^{++}PI^+$	$An^{++}PI^-$ An^+PI^{++}	$An^{++}PI^-$ $An^{++}PI^+$ An^-PI^{++}	$An^{++}PI^-$ $An^{++}PI^+$ An^-PI^{++}	An^-PI^- $An^{++}PI^-$ $An^{++}PI^+$ An^-PI^{+++}

A^n: $AuNP^{negative}$; An: Annexin; A^p: $AuNP^{positive}$; E^n: $ethanol^{negative}$; E^p: $ethanol^{positive}$; PI: Propidium iodide; Superscripts: $^-$within control range, $^+$ > 10% to 15% increase, $^{++}$ > 15% to 30% increase and $^{+++}$ > 30% increase.

($AuNP_{KG}$ dose 20 mg/L) cells exhibited $An^{++}PI^-$ phenotypes, while A^p/E^p ($AuNP_{KG}$ 60 and 100 mg/L) cells exhibited $An^{++}PI^-$, $An^{+++}PI^-$, $An^{++}PI^+$ and An^-PI^{+++} phenotypes. The cell phenotypes in A^p/E^p cells exposed to other AuNPs are shown in (Table 2).

Time-course (20 mg/L data): Distribution of cell phenotypes at different time intervals after ethanol exposure in A^n/E^p and A^p/E^p ($AuNP_{KG}$ dose 20 mg/L) cells are shown in Figure 12. At day-16, A^n/E^p cells exhibited $An^{+++}PI^-$, $An^{++}PI^-$, An^+PI^{++} and An^-PI^{+++} phenotypes, while A^p/E^p ($AuNP_{KG}$ dose 20 mg/L) cells exhibited $An^{+/-}PI^-$ phenotypes, suggesting that a 20 mg/L dose of $AuNP_{KG-50}$ protected against ethanol toxicity. The data for other NPs are not shown since they provided poor protection against ethanol toxicity (Figure 11, Figure 12 and Table 2).

NFκB activation: Figure 13A shows typical gel images of NFκB's (p65-p50)-DNA complex by the fluorescent EMSA. The specificity of the DNA-binding protein was confirmed by competition experiments in which the formation of protein-DNA complex was specifically competed by non-labeled specific probe and by different amounts of nuclear proteins. Figure 13B shows fluorescence intensity of NFκB-DNA band. In the absence of ethanol, a 5, 10, 20 or 40 mg/L dose of $AuNP_{KG-50}$ did not modulate, while 60 mg/L and 100 mg/L dose significantly activated p65-p50. Ethanol exposure, in the absence of AuNPs gradually increased NFκB activation that peaked at day-8. At day-16, the values either did not change or decreased slightly. The 5 and 10 mg/L dose of $AuNP_{KG-50}$ did not, while the 20 mg/L and 40 mg/L doses significantly attenuated NFκB activation by ethanol, thus protecting the cells against the ethanol's adverse effects. Higher AuNP doses augmented NFκB activation and ensuing toxicity by ethanol (Figure 13).

Formation of intracellular protein-corona: Figure 14A shows electrophoretic separation of cytosolic and

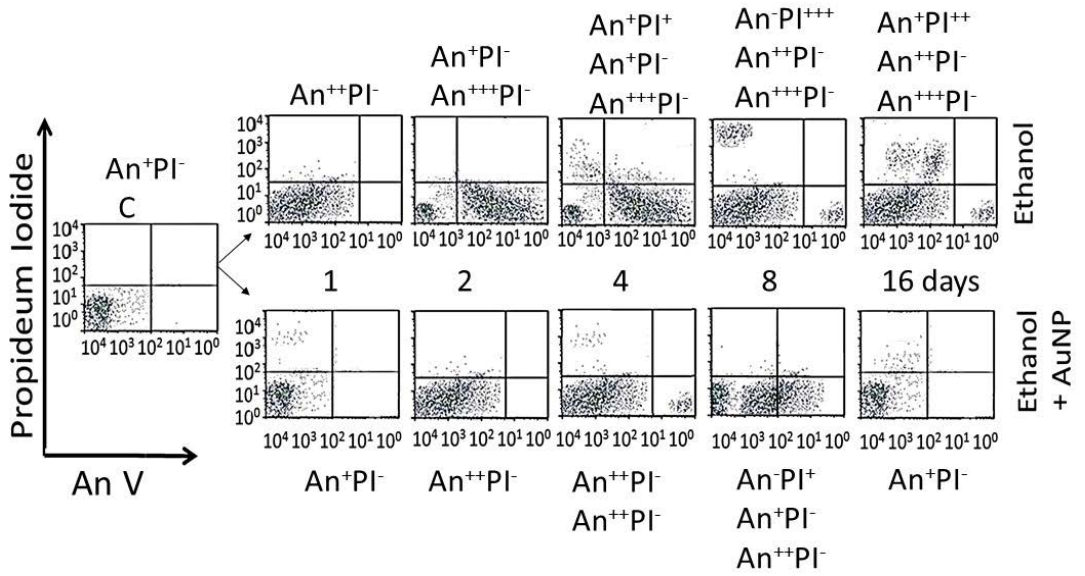

Figure 12: The time-course of incorporation of annexin V and propidium iodide in A^n/E^n cells (C), A^p/E^n cells (bottom, 1 to 16 days, fixed AuNP dose of 20 mg/L), A^p/E^p cells (top, 1 to 16 days, fixed AuNP dose of 20 mg/L) and A^n/E^p cells (top day-1) cells.

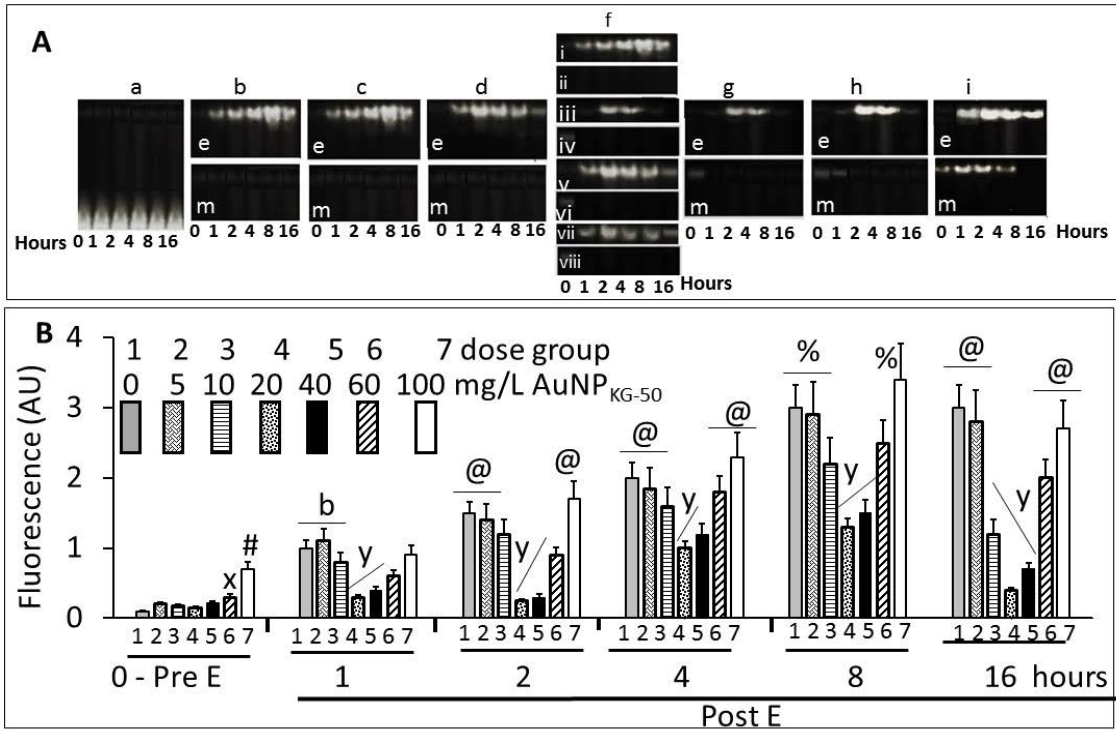

Figure 13: A: Typical electrophoretic separation of NFkB dimer, p65-p50, in A^n/E^n (matrix), A^n/E^p (E+matrix), A^p/E^p (E + 5 to 100 mg/L, data for $AuNP_{KG-50}$ is shown), and A^p/E^n (saline + 5 to 100 mg/L, data for $AuNP_{KG-50}$ is shown) cells. *[a]* matrix exposed control, A^n/E^n cells, *[be]* AuNP negative but ethanol positive A^n/E^p cells, *[bm]* AuNP and ethanol negative A^n/E^n cells, *[ce]* A^p/E^p cells receiving 5 mg/L $AuNP_{KG-50}$, *[cm]* A^p/E^n cells receiving 5 mg/L $AuNP_{KG-50}$, *[de]* A^p/E^p cells receiving 10 mg/L $AuNP_{KG-50}$, *[dm]* A^p/E^n cells receiving 10 mg/L $AuNP_{KG-50}$, [f] A^p/E^p cells receiving 20 mg/L $AuNP_{PEG+K+G}$ (fi), $AuNP_{KG-50}$, (fiii), $AuNP_{K-50}$ (fv) and $AuNP_{G-50}$ (fvii), and *[ge, he, ie]* A^p/E^p cells receiving 40, 60 and 100 mg/L, respectively, and *[gm, hm, im]* A^p/E^n cells receiving 40, 60 and 100 mg/L, respectively; B: Scan of the p65-p50 fluorescence - dose-response and time-course studies. [0 - Pre E] A^p/E^n cells were exposed to different doses of $AuNP_{KG-50}$. [1 to 16 days post ethanol exposure]: A^p/E^p cells were exposed to different doses of $AuNP_{KG-50}$ for 4 days then ethanol for 24 hours. Cells were analyzed at, day-1, day-2, day-4, day-8 and day-16 post ethanol. Values are mean ± SD. x: $p < 0.05$ when values for cells exposed to 60 mg/L were compared with cells exposed to lower AuNP doses. #: $p < 0.05$ when values for cells exposed to 100 mg/L were compared with cells exposed to lower AuNP doses. b: $p < 0.05$ when values for cells exposed to 0, 5 and 10 mg/L were significantly higher than the values for cells exposed to higher doses. y: $p < 0.05$ when values for cells exposed to 20 and 40 mg/L were compared with other values. @: $p < 0.05$ when values for same AuNP dose collected at different time intervals were compared. Values are mean ± SD, n = 5.

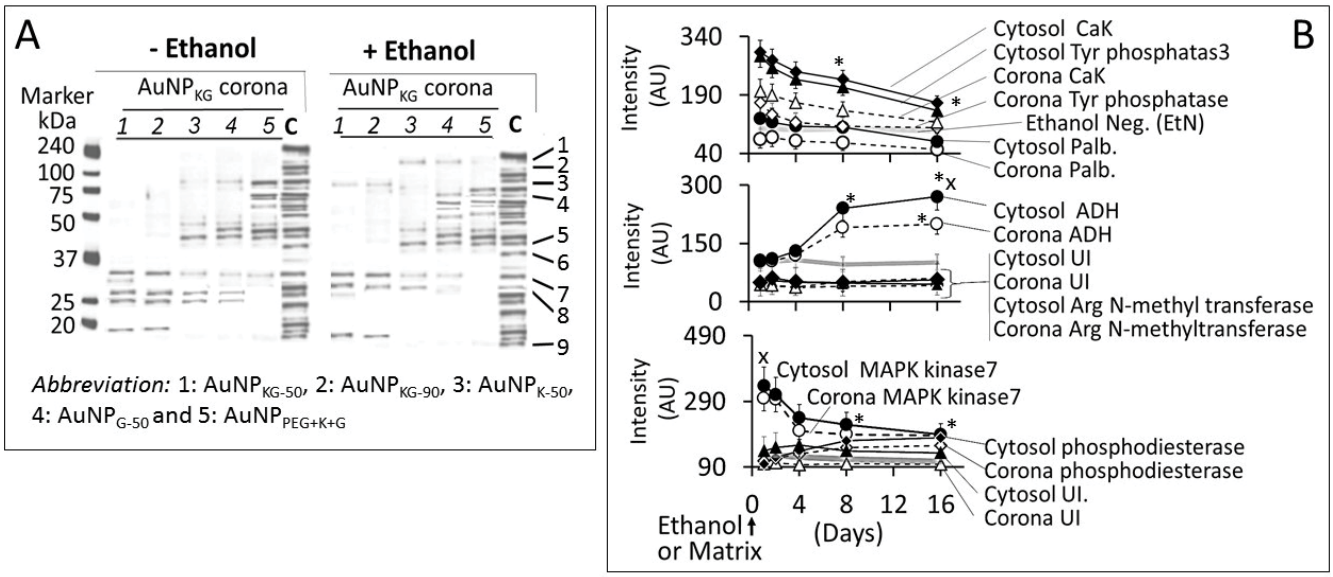

Figure 14: Possible mechanism proposed for uptake and accumulation of AuNPs in cells. N: nucleus; M: mitochondria; E: endoplasmic reticulum.

AuNP-corona proteins from cells exposed to different AuNP preparations. The cytosol proteins ranged from 240 kDa to < 10 kDa, while the AuNP corona proteins ranged from 100 kDa to < 10 kDa in both control and ethanol-exposed cells. The protein composition exhibited the following differences (Figure 14):

i. Out of 35 proteins detected in control (A^n/E^n) cells, 9 cytosolic proteins were confirmed. Tyr phosphorylase, Arg N-methyl transferase and MAPK kinase-7 yielded stronger bands (scan density 2.2 to 2.6) than parvalbumin, ADH, Glu-CoA dehydrogenase, cAMP/gAMP phosphodiesterase, transferrin and casein kinase 1γ2 (scan density 0.3 to 1.4). Day-1 to day-16 values did not differ significantly.

ii. The AuNP corona protein/cytosol protein ratio for Tyr phosphorylase, Arg N-methyl transferase and MAPK kinase-7 increased from < 10 at day-1 to > 20 at day-16. The ratio for other proteins either did not change or increased slightly.

iii. Ethanol exposure did not significantly alter the protein scan values, but significantly suppressed the AuNP corona protein/cytosol protein ratio. Ethanol specifically altered binding of MAPK kinase-7, casein kinase, Tyr phosphorylase and cAMP/gAMP phosphodiesterase to AuNPs, possibly by altering their concentrations in the cytosol. This suggests that ethanol exposure may have directly affects the AuNP-protein interaction.

iv. The composition of protein corona changed temporally. AuNPs extracted from day-1 and day-2 A^n/E^n or A^n/E^p cells interacted with smaller (< 37 kDa) proteins, while AuNPs extracted from day-4 to day-16 cells interacted with proteins ranging from < 37 kDa to 150 kDa. The band intensity increases with increasing incubation time (Figure 14).

Discussion

The present study showed that aqueous extracts of kudzu root and edible gum provided a simple one-step synthesis of AuNPs that had many advantages over the traditional synthesis method. The AuNPs were well dispersed and retained the advantages, while minimizing the disadvantages of the medicinal plant extract. The following sections describe the characteristics and medicinal properties and of AuNPs synthesized by Kudzu root and gum extracts.

Synthesis and characterization of AuNPs

AuNP size, UV absorption and FTIR spectroscopy: The UV-spectra of AuNPs indicated sharp absorption maxima at around 526 to 586 nm, a characteristic absorbance for AuNPs arising possibly due to an interaction of electromagnetic radiations with surface Plasmon of AuNPs. Like the observations of Amendola and Meneghetti [41], the present study also showed that AuNPs synthesized in this study exhibited considerable differences around 200-586 nm, but no differences after the Surface Plasmon Resonance (SPR) region around 500 to 600 nm [42]. In general, absorption maxima around 526 to 586 nm are determined by the AuNP size and incubation temperature. AuNPs of 22, 48 and 99 nm diameter, respectively, exhibited absorption maxima at 520, 540, 533 and 575 nm. Temperature affected UV absorption of AuNPs in a size dependent manner: smaller nanoparticles (< 20 nm diameter) were relatively resistant to temperature changes, while an increase in size is asso-

ciated with an increase in temperature sensitivity [43]. The present study indicated that AuNPs synthesized at different temperatures exhibited differences in the absorption maxima. More research is needed to explain this divergence.

Figure 3 show the FTIR spectra for gum extract, kudzu extract and $AuNP_{KG-50}$. Gum extract exhibit the absorption bands at (i) 3246 cm^{-1} possibly due to the O-H stretching band; (ii) 2901 cm^{-1} due to aliphatic C-H stretching; (iii) 1442, 1374 and 1339 cm^{-1} due to C-H bending vibrations; (iv) 1220 to 998 cm^{-1} due to C-H and O-H deformation and (v) 1145 to 554 cm^{-1} due to the C-O and C-C groups' vibration modes [44]. These bands characterize the carbohydrates present in gum solution. Kudzu extract exhibited broad band between 3600 and 3000 cm^{-1} that is assigned to O-H stretching and to H-bonding involving the -OH groups. The band at 2920 cm^{-1} is assigned to CH_2 symmetrical stretching vibrations. The band at 1639 cm^{-1} is attributed to the scissoring of two O-H bonds, while the bands at 750 cm^{-1} are due to skeletal stretching vibrations. The FTIR spectra for $AuNP_{KG-50}$ (synthesized by kudzu-gum mixture at 50 °C) exhibited bands at 3306 cm^{-1} assigned to O-H stretching vibration of alcohols and phenols, 1630 cm^{-1} assigned to C=O stretching vibration of tertiary amides, 1206 cm^{-1} assigned to C-C-O stretching of epoxy rings and 1044 cm^{-1} assigned to C=O stretching of primary alcohol [43]. From these observations, it is clear the poly-phenols present in the extract are responsible for the reduction and stabilization (Figure 3). The observation that FTIR spectra for $AuNP_{KG-50}$ contains bands that are also present in kudzu and gum extracts suggests that the many of the kudzu and gum ingredients are adsorbed onto the AuNP surface (Table 3).

Characterization of surface ligands: An important observation of this study was that the two MS methods, LDI-TOF-MS and low matrix MALDI-TOF-MS, detected different sets of surfaces and ligands: low-matrix MALDI detected the AuNPs surface charge, while LDI-TOF-MS detected the desorbed organic ligands including an internal standard added to the plant extract. The identities of the ligands were confirmed by analyzing a mixture of authentic standards by the same method. As shown in Figure 4, $AuNP_{KD-50}$ contained the components of kudzu extract (daidzein, puerarin and kakkasaponin III), gum (arabinose, galactose and fructose) and the internal standard (d4-daidzein). The intensity of natural and d4 daidzein did not significantly change during 16 days of cell maintenance. The internal standard allowed semi-quantitative determination of ligand concentrations onto the AuNP surface. This allowed determination of ligand dose as well as the extent of ligand depletion. Earlier studies have shown that puerarin, a naturally occurring isoflavone C-glycosides found in the roots of *Pueraria lobata* and *P. thomsonni* are widely used in China and India for the treatment of alcoholism, cerebrovascular and cardiovascular diseases [45]. Dietary gum is exhibits anti-inflammatory and anti-oxidative properties [46]. Thus, the AuNP's surface ligands may be responsible for beneficial effects reported for the phytochemical-synthetized AuNPs.

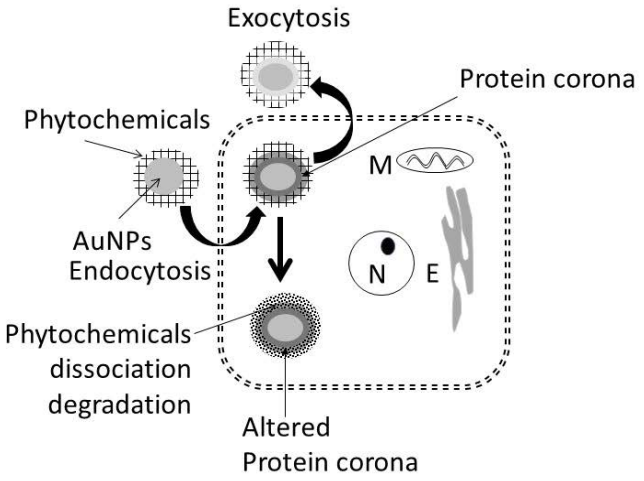

Figure 15: Characterization of protein corona on AuNP surface (A) Effects of ethanol exposure on composition of corona proteins.

Abbreviation: 1: $AuNP_{KG-50}$; 2: $AuNP_{KG-90}$; 3: $AuNP_{K-50}$; 4: $AuNP_{G-50}$ and 5: $AuNP_{PEG+K+G}$. Protein identification: 1: Alcohol dehydrogenase; 2: cAMP/cGMP phosphodiesterase; 3: Tyr phosphatase; 4: Transferring; 5: Glutamate CoA phosphodiesterase; 6: Arginine N-methyltransferase; 7: Casein kinase; 8: MAPK kinase; 9 and 10: Parvalbumin.

(B) Time-course of change in individual protein concentrations in cytosol and desorbed from $AuNP_{KG-50}$.

Table 3: Description of FTIR peaks.

Peak cm^{-1}	Functional group/vibration mode
750	Aromatic protons
927	C-O-C vibration modes of α-1,4 glycosidic linkage
1040/1162	Carbonyl (C=O) group, C-O stretching alcohols (primary, secondary and tertiary), carboxylic acids, esters and ethers
1020/1079 1116/1156	C-O/C stretching in exo/endo-cyclic bonds and C-O-H/C deformation modes of oligo/polysaccharides and absorption bands for carbohydrates
1383/1456	The spectral bands for C-O-H stretching in pyranose and C-H deformation in esters
1621/1637	Aromatic C=C/C-OH stretching in exocyclic bond
2923	Glucoside ring due to the stretching vibration of O-H
3420	O-H, as also the H-bonded alcohols and phenols, carboxylic acid

Cellular uptake and extrusion of AuNPs

Figure 15 shows uptake, fate and extrusion of AuNP in cells. NPs, upon encountering cell membranes, interact with (i) Caveolin-receptors targeted by small AuNPs (5 nm > 20 nm >>50 nm), (ii) Clathrin-receptors for non-phagocytic uptake targeted by relatively larger AuNPs (50 nm) in the absence of serum, and (iii) Scavenger-receptor that mediated phagocytic uptake targeted by relatively larger AuNPs (50 nm) in the absence of serum [46-50] (Figure 15).

Once internalized, NPs either enter the cytosol directly and interact with cytosol-proteins [49] or trapped in endosome-lysosomes complex for processing (NP de functionalization, protein hydrolysis and surface modification) before being transported to the cytosol and the cell's periphery for extrusion via exocytosis [47,51-53]. In general, the endosomal NPs are extruded within 30 to 60 minutes [54], NPs accumulated in multi-vascular bodies' exits cells within 6 days [55], and microtubule accumulated NPs are extruded constitutively via Golgi apparatus [56]. Internalization of nanoparticles can be modified by surface modification [57,58]. PEG coupling of nanoparticles surface significantly reduced the cytotoxic effects of nanoparticles *in vitro* and *in vivo* [59,60].

The present study showed that AuNP synthesized using different plant extracts and incubation temperature exhibited differences in size ($AuNP_{KG}$ > $AuNP_{K}$ > $AuNP_{G}$ or $AuNP_{PEG}$) and composition of surface ligand. Time-dependent decreases in density of certain ligands were observed (Figure 7). In Ethanol-negative cells, AuNP intake maxed within 3 days and the intracellular NPs concentrations exhibited the following patterns: $AuNP_{KG\text{-}90\ and\ -50}$ > $AuNP_{KG\text{-}37}$, > $AuNP_{K\text{-}90,\ 050,\ -37}$ > $AuNP_{G}$ or $AuNP_{PEG+K+G.}$ After discontinuation of NPs, the iAuC decreased gradually and returned to basal level within 16 days. Earlier studies have shown that AuNPs and other NPs are internalized by cells in a size- and surface-dependent manner through (i) Caveolin-mediated uptake targeted by small AuNPs (5 nm > 20 nm >> 50 nm), (ii) Clathrin-mediated non-phagocytic uptake targeted by relatively larger AuNPs (50 nm) in the absence of serum, and (iii) Scavenger-receptor mediated phagocytic uptake targeted by relatively larger AuNPs (50 nm) in the absence of serum [46-50]. Since SH SY-5Y are non-phagocytic, they may be internalized via caveolin-mediated and clathrin-mediated endocytosis. This suggests that, unlike the AuNPs uptake that varied according to the synthesis procedure, their excretion from the cells did not differ significantly.

In ethanol-positive cells, harvested at 1, 2, 4 and 8 days after ethanol discontinuation, iAuCs were either significantly lower than (as for $AuNP_{KG}$ and $AuNP_{PEG}$ pretreated cells) or comparable to (as for $AuNP_{K}$ or $AuNP_{G}$ pretreated cells) the corresponding values in ethanol-negative cells. At day-16, the two cell groups exhibited comparable values. This suggests that ethanol may differentially affect internalization of AuNPs that may be associated with unique properties of ethanol. Earlier studies have shown that ethanol, due to their polar and nonpolar characteristics, can (i) Leak through the cell membrane and form hydrogen-bonds with phospholipids head-group that disrupts the hydrophobic chain orientation and (ii) Increases the membrane fluidity by denaturing proteins and affecting the lipids, resulting in formation of small holes in the membrane [50,61,62]. Ethanol, by forming H-bonds may orient the phospholipids outwards, thus increasing their movement and the membrane fluidity increases and affecting the integrity of the membrane receptors [63]. Therefore, $AuNP_{KG}$, being relatively smaller nanoparticles, may escape the cells via exiting through the ethanol-induced membrane holes.

Toxicity of plant-extract synthesized AuNPs

Although surface functionalized AuNPs, because of their unique properties, have emerged as promising candidates for biomedical applications such as sensing, imaging, and drug delivery [64], their application in clinical setting has not materialized due to uncertainties in their adverse effects. Since the NP toxicity is impacted by their size, shape, charge and surface functionalization, toxicity of each individual NP preparation must be evaluated before testing the beneficial effects. The present study showed that a 5 to 20 mg/L dose of AuNP preparations did not significantly affect (i) Viable cell enumeration; (ii) LDH and lipid peroxidase activities; (iii) NFκB activation and (iv) Apoptotic/necrotic cell enumerations. However, 40 to 100 mg/L dose caused a dose-dependent increase in these indices. This suggests that relatively higher doses (> 60 mg/L) of AuNPs may cause different degrees of cytotoxicity in SH SY5Y cells. These results are consistent with previous investigations performed with MCF-7, PC-3 and dermal fibroblasts [65,66] which demonstrated that the AuNPs, at higher doses (> 100 mg/L), impaired the proliferation of dermal fibroblasts and induced an abnormal formation of actin filaments, causing therefore a reduced cellular motility and influencing the cell morphology. Vijayakumar, Ganesan [67] reported that citrated and biotinylated 18 nm gold nanoparticles did not induce toxicity, while smaller particles were much more toxic in leukemic K562 cell lines. Similar results were reported by Cho, et al. [68] in adeno-carcinomic human alveolar basal epithelial cell line, A549. These observations suggest that a 5 to 20 mg/L dose of AuNPs can be used safely in this experimental setup. However, toxicity must be reevaluated when the NPs physicochemical properties or the experimental conditions change.

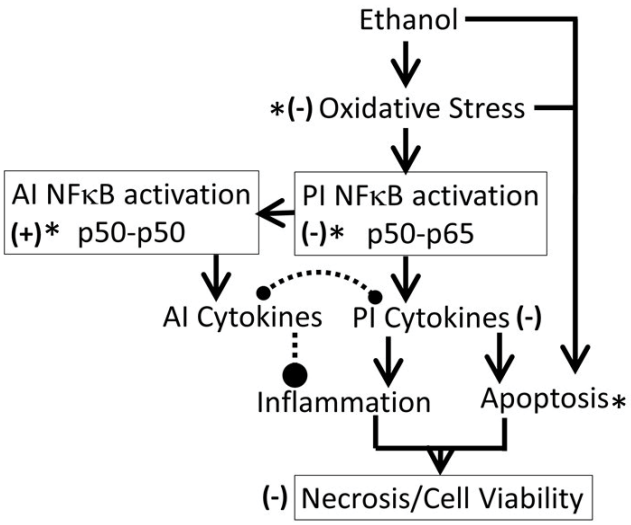

Figure 16: Proposed mechanism for ethanol-induced cytotoxicity. *: proposed target sites for AuNP's protective effects. Solid lines: activation; broken lines: inhibition; (-): inhibitory effects of AuNPs and (+) activation by AuNPs.

Therapeutic potency of plant-extract synthesized AuNPs against ethanol toxicity

Ethanol cytotoxicity: It is well established that acute or chronic ethanol exposure (1) Up-regulated oxidative stress, dysregulated inflammation and cell signaling [20]; (2) Up-regulated expression of cytokines, increased amounts of TNF-α and depleted both cytosolic and mitochondrial GSH that may contribute to an increase in oxidative stress [69]; (3) Significantly inhibited activities of p450 enzymes CYP1A1, CYP2B6, CYP2C19, and CYP2D6 that may alter xenobiotic metabolism and drug pharmacokinetics [70], and (4) Significantly reduced total number of embryonic stem cells, inducing the formation of cardiomyocytes [62]. The present study demonstrated that a 54 mM concentration of ethanol exposure exerted immediate cytotoxicity in SH SY5Y cells possibly via the mechanisms listed above. The cytotoxic effects of ethanol persisted for up to 16 days after the cells were treated with ethanol, suggesting that 24 h ethanol exposure may have long-term cytotoxicity, possibly dysregulating oxidative stress and inflammation (Figure 16).

Protective effects of AuNPs against ethanol toxicity: This study showed that AuNPs synthesized using kudzu and gum extracts protected SH-SY5Y cells against ethanol toxicity, although to different degrees ($AuNP_{KG-90, -50}$: 60 to 80% protection, $AuNP_{KG-37}$, $AuNP_{K-90, -50, -37}$: 30 to 50% protection, $AuNP_{PEG + K + G}$ (20 to 30% protection), and $AuNP_{PEG}$ and $AuNP_{G-50, -90}$ (< 20% protection). The present observations are supported by earlier experimental studies showing that many medicinal plants possessed preventive and therapeutic properties against alcoholism, alcohol withdrawal symptoms and alcohol toxicity [22,25,28,29,71-80]. Earlier studies have shown that high isoflavone contents in kudzu root, *Solanum torvum* fruit, *Cassia tora* leaves, *Atrocarpus altilis* leaves *Angelicae pubescens* extracts may be attributed to their protective effects against ethanol toxicity *in vitro* [81-85]. Despite strong evidence, clinical applications of phytochemicals is hindered by the following major hurdles: (i) Poor solubility and bioavailabity; (ii) Inability to cross the blood-brain barrier and (iii) Lack of plant extract standardization that prohibits accurate determination of dose-response relationships, yielding high variability in results [86]. One of the key problems associated with earlier studies showing protective effects of plant-extract-synthesized NPs is that they did not identify the NPs' surface ligands, thus could not conduct dose-response studies. In the present study, LDI (no matrix) or low-matrix MALDI identified the ligands adsorbed onto the NPs surface. Inclusion of an internal standard allowed standardization of the NPs and provides possibility of conducting dose-response studies for surface ligands.

Possible mechanisms for protection against ethanol: The protective effects of plant-extract-synthesized AuNPs may be attributed to the adsorption of bioactive compounds onto the AuNPs surface. In the present study, the following ligands have been identified from the AuNPs surface (Figure 4):

i. Gum ligands such as arabinose, galactose and fructose that are part of a highly branched polysaccharide (MW 3×10^5) consisting of b-(1-3) galactose backbone with linked branches of arabinose and rhamnose [87]. Ali, et al. [44] have provided direct evidence of anti-inflammatory and anti-oxidative capacities of edible Gum Arabic (GA) that ameliorates superoxide production and DNA double strand breakage. Cuesta, et al. [88] and Faggio, et al. [89] have reported high immune-stimulatory, anti-inflammatory and anti-oxidation properties of GA in mammals and aquatic animals, respectively. Studies [90-93] have also shown that edible gum, in addition to being anti-oxidative; enhance the biocompatibility and bioavailability of AuNPs and other NPs such as AgNPs and Magnetic iron oxide Nanoparticles (MNP). The GA coating offers two major benefits: it enhances colloidal stability and provides reactive functional groups suitable for coupling of bioactive compounds.

ii. Kudzu ligands such as daidzein and puerarin possess potent anti-inflammatory and anti-oxidation properties, thus protecting against alcohol-mediated disorders [28,29,94-97]. As shown in Figure 9, ethanol induces oxidative stress and ensuing downstream activation of p50-p65 (a pro-inflammatory dimer of NFκB) and suppression of p50-p50 (an anti-inflam-

matory dimer of NFκB), resulting in dysregulation of inflammation and activation of pro-apoptosis signaling [32]. The addictive effects of ethanol are mediated by the brain addiction pathways including dopamine, GABA, NMDA, and serotonin neurons [5,98,99]. Earlier studies have shown that kudzu root extract the brain addiction circuits, especially the dopamine, GABA, NMDA and Glu neurons/receptors in protecting the brain against the adverse effects of ethanol and suppressing the severity of the withdrawal symptoms [100-102].

Taken together, these observations suggest that pretreatment of cells with the AuNP-adsorbed plant-components are more potent in protecting the cells against ethanol toxicity than pretreatment of cells with crude plant extracts their purified components.

AuNP-Protein Interaction: It is well established that NPs in biological and environmental media (blood, intracellular fluid, plant extracts or environmental samples) interact with the media components such as soluble proteins, lipids and other ingredients, and form a surface corona that may modulate the NPs' physicochemical and biological (cellular/tissue responses such as cellular uptake, kinetics, signaling, accumulation, transport, and toxicity) properties [103-108]. Formation of protein corona in blood or intracellular fluids may depend upon the composition and organization of surface proteins [109]. In general, the corona may be divided into two components: the "hard" corona with long exchange time and "soft" coronas with short exchange times [109]. In a biological fluid, the surface corona's protein composition, amount and presentation on the surface, modify their beneficial, therapeutic or adverse effects [110-115]. In the present study, 9 proteins, ranging from < 10 to 200 kDa, have been identified in cytosol and hard-corona of AuNPs synthesized using different plant extracts and incubation temperature (Figure 14A). $AuNP_{KG-50}$ (average diameter - 8 nm), $AuNP_{K-50}$ (average diameter - 39 nm) and $AuNP_{G-50}$ (average diameter - 41) interacted with protein < 37 kDa, 50 to 37 kDa and > 75 kDa, respectively. This suggests that the size and surface ligand composition may determine the composition of proteins corona. As shown in Figure 14B, the time-course of change in individual corona proteins paralleled the change in corresponding cytosol proteins, suggesting the possibility of rapid exchange between corona and cytosol. It is hypothesized that poor protein-binding capacity of $AuNP_{KG-50}$ may contribute to its high therapeutic activity and relatively lower toxicity.

Conclusion

Although kudzu extract, edible gum extract and a combination of both ($AuNP_{KG-37, -50, -90}$) incubated at 37 °C, 50 °C and 75 °C, reduced Au^{3+} into colloidal gold nanoparticles (kudzu synthesized: $AuNP_{K-50, -90, -37}$, gum synthesized: $AuNP_{G-50, G-90}$, and kudzu+gum synthesized: $AuNP_{KG-37, -50, -90}$), they differed in size ($AuNP_{KG}$ << $AuNP_{K}$ < $AuNP_{G}$) and physicochemical properties, including their interaction with cytosol proteins ($AuNP_{KG}$ << $AuNP_{K}$ < $AuNP_{G}$). The surface of each AuNP contained the extract's active ingredients that were analyzed and confirmed using LDI and low-matrix MALDI. $AuNP_{KG-50}$ was least toxic to SH-SY5Y cells and most effective in suppressing the adverse effects of ethanol on SH-SY5Y cells. The beneficial and adverse effects of AuNPs may have been modified by the formation of proteins corona.

References

1. Sacks JJ, Roeber J, Bouchery EE, et al. (2013) State costs of excessive alcohol consumption, 2006. Am J Prev Med 45: 474-485.
2. Kelly JF (2017) Are societies paying unnecessarily for an otherwise free lunch? Final musings on the research on Alcoholics Anonymous and its mechanisms of behavior change. Addiction 112: 943-945.
3. Rabiee R, Agardh E, Coates MM, et al. (2017) Alcohol-attributed disease burden and alcohol policies in the BRICS–countries during the years 1990-2013. J Glob Health 7.
4. Stahre M, Roeber J, Kanny D, et al. (2014) Contribution of excessive alcohol consumption to deaths and years of potential life lost in the United States. Preventing Chronic Disease 11.
5. Koob GF (2008) A role for brain stress systems in addiction. Neuron 59: 11-34.
6. Koob GF, Volkow ND (2010) Neurocircuitry of addiction. Neuropsychopharmcology 35: 217-238.
7. Singh AK (2017) Critical Review of Alcohol, Alcoholism and the Withdrawal Symptoms I. Mechanisms of Addiction and Withdrawal Syndrome. The Scientific Pages of Addiction and Rehabilitation.
8. Ducharme LJ, Chandler RK, Harris AH (2016) Implementing Effective Substance Abuse Treatments in General Medical Settings: Mapping the Research Terrain. Journal of Substance Abuse Treatment 60: 110-118.
9. Singh AK (2017) Critical Review of Alcohol, Alcoholism and the Withdrawal Symptoms II. Treatment Strategies. The Scientific Pages of Addiction and Rehabilitation.
10. Litten RZ, Bradley AM, Moss HB (2010) Alcohol biomarkers in applied settings: Recent advances and future research opportunities. Alcohol Clin Exp Res 34: 955-967.
11. Carai MA, Agabio R, Bombardelli E, et al. (2000) Potential use of medicinal plants in the treatment of alcoholism. Fitoterapia 71: S38-S42.
12. Taritatu DV, Bagade VB, Karambelkar PJ, et al. (2013) Natural Bioenhancers: An overview. Journal of Pharmacognosy and Phytochemistry 2: 55-60.
13. Zhou J, Ralston J, Sedev R, et al. (2009) Functionalized gold nanoparticles: synthesis, structure and colloid stability. J Colloid Interface Sci 331: 251-262.

14. Haiss W, Thanh NT, Aveyard J, et al. (2007) Determination of size and concentration of gold nanoparticles from UV−Vis spectra. Anal Chem 79: 4215-4221.

15. Singh AK, Jiang Y, Gupta S, et al. (2013) Anti-inflammatory potency of nano-formulated puerarin and curcumin in rats subjected to the lipopolysaccharide-induced inflammation. J Med Food 16: 899-911.

16. Kumar PK, Paul W, Sharma CP (2011) Green synthesis of gold nanoparticles with Zingiber officinale extract: Characterization and blood compatibility. Process Biochemistry 46: 2007-2013.

17. Nellore J, Pauline C, Amarnath K, et al. (2012) Antioxidant effect of gold nanoparticles synthesised from curcuma longa restrains 1-methyl-2-phenyl pyridinium ion induced stress in PC12 cells. Journal of Nanoneuroscience 2: 63-74.

18. Khadeeja Parveen, Viktoria Banse, Lalita Ledwani (2016) Green synthesis of nanoparticles: Their advantages and disadvantages. AIP Conference Proceedings 1724.

19. Patra JK, Baek KH (2014) Green Nanobiotechnology: Factors Affecting Synthesis and Characterization Techniques. Journal of Nanomaterials 2014: 417305.

20. Elia P, Zach R, Hazan S, et al. (2014) Green synthesis of gold nanoparticles using plant extracts as reducing agents. Int J Nanomedicine 9: 4007-4021.

21. Khan AU, Yuan Q, Wei Y, et al. (2016) Photocatalytic and antibacterial response of biosynthesized Gold nanoparticles. J Photochem Photobiol B 162: 273-277.

22. Tahir K, Nazir S, Ahmad A, et al. (2017) Facile and green synthesis of phytochemicals capped platinum nanoparticles and in vitro their superior antibacterial activity. J Photochem Photobiol B 166: 246-251.

23. Tahir K, Nazir S, Li B, et al. (2015) Enhanced visible light photocatalytic inactivation of Escherichia coli using silver nanoparticles as photocatalyst. J Photochem Photobiol B 153: 261-266.

24. Tahir K, Ahmad A, Li B, et al. (2016) Visible light photo catalytic inactivation of bacteria and photo degradation of methylene blue with Ag/TiO2nanoompsite prepared by a novel method. J Photochem Photobiol B 162: 189-198.

25. Tahir K, Nazir S, Li B, et al. (2016) *Sapium sebiferum* leaf extract mediated synthesis of palladium nanoparticles and in vitro investigation of their bacterial and photocatalytic activities. J Photochem Photobiol B 164: 164-173.

26. Tahir K, Ahmad A, Li B, et al. (2016) Preparation, characterization and an efficient photocatalytic activity of Au/TiO 2 nanocomposite prepared by green deposition method. Materials Letters 178: 56-59.

27. Ahmad A, Wei Y, Syed F, et al. (2016) *Isatis tinctoria* mediated synthesis of amphotericin B-bound silver nanoparticles with enhanced photoinduced antileishmanial activity: A novel green approach. J Photochem Photobiol B 161: 17-24.

28. Khan FU, Chen Y, Khan NU, et al. (2017) Visible light inactivation of E. coli, Cytotoxicity and ROS determination of biochemically capped gold nanoparticles. Microbiol Pathogenesis 107: 419-424.

29. Khan AU, Yuan Q, Wei Y, et al. (2016) Longan fruit juice mediated synthesis of uniformly dispersed spherical AuNPs: cytotoxicity against human breast cancer cell line MCF-7, antioxidant and fluorescent properties. RSC Advances 6: 23775-23782.

30. Khan AU, Yuan Q, Wei Y, et al. (2016) Ultra-efficient photocatalytic deprivation of methylene blue and biological activities of biogenic silver nanoparticles. J Photochem Photobiol B 159: 49-58.

31. Khan ZUH, Khan A, Shah A, et al. (2016) Enhanced photocatalytic and electrocatalytic applications of green synthesized silver nanoparticles. Journal of Molecluar Liquids 220: 248-257.

32. Khan FU, Chen Y, Khan NU, et al. (2016) Antioxidant and catalytic applications of silver nanoparticles using Dimocarpus longan seed extract as a reducing and stabilizing agent. J Photochem Photobiol B 164: 344-351.

33. Benlhabib E, Baker JI, Keyler JE, et al. (2004) Kudzu root extract suppresses voluntary alcohol intake and alcohol withdrawal symptoms in P rats receiving free access to water and alcohol. J Med Food 7: 168-179.

34. Benlhabib E, Baker JI, Keyler DE, et al. (2004) Effects of purified puerarin on voluntary alcohol intake and alcohol withdrawal symptoms in P rats receiving free access to water and alcohol. J Med Food 7: 180-186.

35. Ali BH, Al-Husseni I, Beegam S, et al. (2013) Effect of Gum Arabic on Oxidative Stress and Inflammation in Adenine–Induced Chronic Renal Failure in Rats. PLoS One 8: e55242.

36. Pedersen SM, Graabaek PM (1977) A unified method for the determination of gold in biological fluids by flameless atomic absorption spectroscopy. Scand J Clin Lab Invest 37: 91-94.

37. Buege JA, Aust SD (1978) Microsomal lipid peroxidation. Methods Enzymol 52: 302-310.

38. Chan FK, Moriwaki K, De Rosa MJ (2013) Detection of necrosis by release of lactate dehydrogenase activity. Methods Mol Biol 979: 65-70.

39. Singh AK, Jiang Y (2004) Differential activation of NFκB/RelA-p50 and NFκB/p50-p50 in control and alcohol-drinking rats subjected to carrageenin-induced pleurisy. Mediators of Inflammation 13: 255-262.

40. Singh AK, Gupta S (2007) Analysis of recombinant human erythropoietin and darbepoietin in spiked plasma. Proteomics - Clinical Applications 1: 626-639.

41. Amendola V, Meneghetti M (2009) Laser ablation synthesis in solution and size manipulation of noble metal nanoparticles. Phys Chem Chem Phys 11: 3805-3821.

42. Ghosh SK, Pal T (2007) Interparticle coupling effect on the surface plasmon resonance of gold nanoparticles: from theory to applications. Chem Rev 107: 4797-4862.

43. Noguez C (2007) Surface plasmons on metal nanoparticles: the influence of shape and physical environment. The Journal of Physical Chemistry C 111: 3806-3819.

44. Dyal C, Nguyen N, Hadden J, et al. (2006) Green synthesis of gold and silver nanoparticles from plant extracts. The Am Chem Soc 231.

45. Kora AJ, Beedu SR, Jayaraman A (2012) Size-controlled green synthesis of silver nanoparticles mediated by gum ghatti (Anogeissus latifolia) and its biological activity. Org Med Chem Lett 2: 17.

46. Zhao K, Penttinen P, Guan T, et al. (2011) The diversity and anti-microbial activity of endophytic actinomycetes isolated from medicinal plants in Panxi plateau, China. Curr Microbiol 62: 182-190.

47. Chithrani BD, Ghazani AA, Chan WC (2006) Determining the size and shape dependence of gold nanoparticle uptake into mammalian cells. Nano Lett 6: 662-668.

48. Chithrani BD, Chan WC (2007) Elucidating the mechanism of cellular uptake and removal of protein-coated gold nanoparticles of different sizes and shapes. Nano Lett 7: 1542-1550.

49. Alkilany AM, Murphy CJ (2010) Toxicity and cellular uptake of gold nanoparticles: what we have learned so far? J Nanopart Res 12: 2313-2333.

50. Ma X, Wu Y, Jin S, et al. (2011) Gold nanoparticles induce autophagosome accumulation through size-dependent nanoparticle uptake and lysosome impairment. ACS Nano 5: 8629-8639.

51. Worley SL, Vaughn BJ, Terry AI, et al. (2015) Time- and dose-dependent effects of ethanol on mouse embryonic stem cells. Reprod Tocicol 57: 157-164.

52. Mukherjee S, Ghosh RN, Maxfield FR (1997) Endocytosis. Physiological Reviews 77: 759-803.

53. Chithrani DB, Jelveh S, Jalali F, et al. (2010) Gold nanoparticles as radiation sensitizers in cancer therapy. Radiat Res 173: 719-728.

54. Kam NW, Liu Z, Dai H (2006) Carbon nanotubes as intracellular transporters for proteins and DNA: an investigation of the uptake mechanism and pathway. Angew Chem Int Ed Engl 45: 577-581.

55. Wilhelm C, Gazeau F, Roger J, et al. (2002) Interaction of anionic superparamagnetic nanoparticles with cells: kinetic analyses of membrane adsorption and subsequent internalization. Langmuir 18: 8148-8155.

56. Oh N, Park JH (2014) Endocytosis and exocytosis of nanoparticles in mammalian cells. Int J Nanomedicine 9: 51-63.

57. Sakhtianchi R, Minchin RF, Lee KB, et al. (2013) Exocytosis of nanoparticles from cells: role in cellular retention and toxicity. Adv Colloid Interface Sci 201: 18-29.

58. Murphy CJ, Gole AM, Stone JW, et al. (2008) Gold nanoparticles in biology: beyond toxicity to cellular imaging. Acc Chem Res 41: 1721-1730.

59. Khlebtsov N, Dykman L (2011) Biodistribution and toxicity of engineered gold nanoparticles: a review of in vitro and in vivo studies. Chem Soc Rev 40: 1647-1671.

60. Lee KC, Lin SJ, Lin CH, et al. (2008) Size effect of Ag nanoparticles on surface plasmon resonance. Surface and Coatings Technology 202: 5339-5342.

61. Chompoosor A, Saha K, Ghosh PS, et al. (2010) The role of surface functionality on acute cytotoxicity, ROS generation and DNA damage by cationic gold nanoparticles. Small 6: 2246-2249.

62. Aratono M, Toyomasu T, Villeneuve M, et al. (1997) Thermodynamic study on the surface formation of the mixture of water and ethanol. Journal of Colloid and Interface Science 191: 146-153.

63. Holte LL, Gawrisch K (1997) Determining ethanol distribution in phospholipid multilayers with MAS- NOESY spectra. Biochemistry 36: 4669-4674.

64. Patra M, Salonen E, Terama E, et al. (2006) Under the influence of alcohol: the effect of ethanol and methanol on lipid bilayers. Biophys J 90: 1121-1135.

65. Peer D, Karp JM, Hong S, et al. (2007) Nanocarriers as an emerging platform for cancer therapy. Nature Nanotechnology 2: 751-760.

66. Pernodet N, Fang X, Sun Y, et al. (2006) Adverse effects of citrate/gold nanoparticles on human dermal fibroblasts. Small 2: 766-773.

67. Connor EE, Mwamuka J, Gole A, et al. (2005) Gold nanoparticles are taken up by human cells but do not cause acute cytotoxicity. Small 1: 325-327.

68. Vijayakumar S, Ganesan S (2012) In vitro cytotoxicity assay on gold nanoparticles with different stabilizing agents. Journal of Nanomaterials 2012: 734398.

69. Choi SY, Jeong S, Jang SH, et al. (2012) In vitro toxicity of serum protein-adsorbed citrate-reduced gold nanoparticles in human lung adenocarcinoma cells. Toxicol In Vitro 26: 229-237.

70. Neuman MG, Shear NH, Bellentani S, et al. (1998) Role of cytokines in ethanol-induced cytotoxicity in vitro in Hep G2 cells. Gastroenterology 115: 157-166.

71. Busby WF, Ackermann JM, Crespi CL (1999) Effect of methanol, ethanol, dimethyl sulfoxide, and acetonitrile on in vitro activities of cDNA-expressed human cytochromes P-450. Drug Metab Dispos 27: 246-249.

72. Prince PSM, Menon VP, Gunasekaran G (1999) Hypolipidaemic action of Tinospora cordifolia roots in alloxan diabetic rats. J Ethnopharmacol 64: 53-57.

73. Prince SMP, Menon VP (2003) Hypoglycaemic and hypolipidaemic action of alcohol extract of Tinospora cordifolia roots in chemical induced diabetes in rats. Phytother Res 17: 410-413.

74. Perfumi M, Ciccocioppo R, Angeletti S, et al. (1999) Effects of Hypericum perforatum extract on alcohol intake in Marchigian Sardinian alcohol-preferring rats. Alcohol Alcohol 34: 690-698.

75. Overstreet DH, Keung WM, Rezvani AH, et al. (2003) Herbal remedies for alcoholism: promises and possible pitfalls. Alcohol Clin Exp Res 27: 177-185.

76. Shati AA, Elsaid FG (2009) Effects of water extracts of thyme (Thymus vulgaris) and ginger (Zingiber officinale Roscoe) on alcohol abuse. Food Chem Toxicol 47: 1945-1949.

77. Tomczyk M, Zovko-Koncic M, Chrostek L (2012) Phytotherapy of alcoholism. Nat Prod Commun 7: 273-280.

78. Ozarowski M, Mikolajczak PL, Thiem B (2013) Medicinal plants in the phytotherapy of alcohol or nicotine addiction. Implication for plants in vitro cultures. Przegl Lek 70: 869-874.

79. Otunola GA, Afolayan AJ (2016) Therapeutic effect of aqueous extracts of three dietary spices and their mixture on lipid metabolism and oxidative stress in a rat model of chronic alcohol consumption. Pak J Pharm Sci 29: 1155-1161.

80. Sharma B, Dabur R (2016) Protective Effects of Tinospora cordifolia on Hepatic and Gastrointestinal Toxicity Induced by Chronic and Moderate Alcoholism. Alcohol Alcohol 51: 1-10.

81. Shirolkar A, Sharma B, Lata S, et al. (2016) Guduchi Sawras (Tinospora cordifolia): An Ayurvedic drug treatment modulates the impaired lipid metabolism in alcoholics through dopaminergic neurotransmission and anti-oxidant defense system. Biomed Pharmacother 83: 1265-1277.

82. Ramamurthy C, Padma M, Mareeswaran R, et al. (2013) The extra cellular synthesis of gold and silver nanoparticles and their free radical scavenging and antibacterial properties. Colloids Surf B Biointerfaces 102: 808-815.

83. Saravanakumar A, Ganesh M, Jayaprakash J, et al. (2015) Biosynthesis of silver nanoparticles using Cassia tora leaf extract and its antioxidant and antibacterial activities. Journal of Industrial and Engineering Chemistry 28: 277-281.

84. Ravichandran V, Vasanthi S, Shalini S, et al. (2016) Green synthesis of silver nanoparticles using Atrocarpus altilis leaf extract and the study of their antimicrobial and antioxidant activity. Material Letters 180: 264-267.

85. Wang C, Mathiyalagan R, Kim YJ, et al. (2016) Rapid green synthesis of silver and gold nanoparticles using Dendropanax morbifera leaf extract and their anticancer activities. Int J Nanomedicine 11: 3691-3701.

86. Markus J, Wang D, Kim YJ, et al. (2017) Biosynthesis, Characterization, and Bioactivities Evaluation of Silver and Gold Nanoparticles Mediated by the Roots of Chinese Herbal Angelica pubescens Maxim. Nanoscale Res Lett 12: 46.

87. Tatiraju DV, Varsha M, Jadhav VK, et al. (2013) Painful Diabetic Neuropathy: Mechanisms to Management. J Adv Pharm Edu Res 3.

88. Dror Y, Cohen Y, Yerushalmi-Rozen R (2006) Structure of gum arabic in aqueous solution. Journal of Polymer Sci Part B Polymer Physics 44: 3265-3271.

89. Cuesta A, Rodríguez A, Esteban MA, et al. (2005) In vivo effects of propolis, a honeybee product, on gilthead seabream innate immune responses. Fish Shellfish Immunol 18: 71-80.

90. Faggio C, Fazio F, Marafioti S, et al. (2015) Oral administration of Gum Arabic: effects on haematological parameters and oxidative stress markers in Mugil cephalus. Iranian Journal of Fisheries Sciences 14: 60-72.

91. Williams DN, Gold KA, Holoman TRP, et al. (2006) Surface modification of magnetic nanoparticles using gum arabic. Journal of Nanoparticle Research 8: 749-753.

92. Kattumuri V, Katti K, Bhaskaran S, et al. (2007) Gum Arabic as a Phytochemical Construct for the Stabilization of Gold Nanoparticles: In Vivo Pharmacokinetics and X-ray-Contrast-Imaging Studies. Small 3: 333-341.

93. Roque AC, Bicho A, Batalha IL, et al. (2009) Biocompatible and bioactive gum Arabic coated iron oxide magnetic nanoparticles. Journal of Biotechnology 144: 313-320.

94. Wu CC, Chen DH (2010) Facile green synthesis of gold nanoparticles with gum arabic as a stabilizing agent and reducing agent. Gold Bulletin 43: 234-240.

95. Chen X, Li R, Liang T, et al. (2013) Puerarin improves metabolic function leading to hepatoprotective effects in chronic alcohol-induced liver injury in rats. Phytomedicine 20: 849-852.

96. Li R, Zheng N, Liang T, et al. (2013) Puerarin attenuates neuronal degeneration and blocks oxidative stress to elicit a neuroprotective effect on substantia nigra injury in 6-OHDA-lesioned rats. Brain Res 1517: 28-35.

97. Li Z, Shangguan Z, Liu Y, et al. (2014) Puerarin protects pancreatic β-cell survival via PI3K/Akt signaling pathway. J Mol Endocrinol 53: 71-79.

98. Zhao M, Du YQ, Yuan L, et al. (2010) Protective effect of puerarin on acute alcoholic liver injury. Am J Chin Med 38: 241-249.

99. Leshner AI (1997) Addiction is a brain disease, and it matters. Science 278: 45-47.

100. Le Moal M, Koob GF (2007) Drug addiction: pathways to the disease and pathophysiological perspectives. Eur Neuropsychopharmacol 17: 377-393.

101. Terenius L (1998) Rational treatment of addiction. Cur Opin Chem Biol 2: 541-547.

102. Meletis CD, Zabriskie N (2008) Natural approaches to treating addiction. Alt Complementary Ther 14: 275-281.

103. Ma ZZ, Xu W, Jensen NH, et al. (2008) Isoquinoline alkaloids isolated from Corydalis yanhusuo and their binding affinities at the dopamine D1 receptor. Molecules 13: 2303-2312.

104. Casals E, Pfaller T, Duschl A, et al. (2010) Time evolution of the nanoparticle protein corona. ACS Nano 4: 3623-3632.

105. Mahmoudi M, Lynch I, Ejtehadi MR, et al. (2011) Protein-nanoparticle interactions: opportunities and challenges. Chem Rev 111: 5610-5637.

106. Ghavami M, Saffar S, Abd Emamy B, et al. (2013) Plasma concentration gradient influences the protein corona decoration on nanoparticles. RSC Adv 3: 1119-1126.

107. Nel AE, Madler L, Velegol D, et al. (2009) Understanding biophysicochemical interactions at the nano-bio interface. Nat Mater 8: 543-557.

108. Treuel L, Nienhaus GU (2012) Toward a molecular understanding of nanoparticle-protein interactions. Biophysical Reviews 4: 137-147.

109. Walkey CD, Chan WC (2012) Understanding and controlling the interaction of nanomaterials with proteins in a physiological environment. Chem Soc Rev 41: 2780-2799.

110. Monopoli MP, Walczyk D, Campbell A, et al. (2011) Physical− chemical aspects of protein corona: relevance to in vitro and in vivo biological impacts of nanoparticles. Journal of the American Chemical Society 133: 2525-2534.

111. Cedervall T, Lynch I, Foy M, et al. (2007) Detailed identification of plasma proteins adsorbed on copolymer nanoparticles. Angew Chem Int Ed Engl 46: 5754-5756.

112. Landsiedel R, Ma-Hock L, Kroll A, et al. (2010) Testing Metal-Oxide Nanomaterials for Human Safety. Adv Mater 22: 2601-2627.

113. Lundqvist M, Sethson I, Jonsson BH (2004) Protein Adsorption onto Silica Nanoparticles: Conformational Changes Depend on the Particles' Curvature and the Protein Stability. Langmuir 20: 10639-10647.

114. Lundqvist M, Sethson I, Jonsson BH (2005) Transient Interaction with Nanoparticles "Freezes" a Protein in an Ensemble of Metastable Near-Native Conformations. Biochemistry 44: 10093-10099.

115. Karajanagi SS, Vertegel AA, Kane RS, et al. (2004) Structure and Function of Enzymes Adsorbed onto Single-Walled Carbon Nanotubes. Langmuir 20: 11594-11599.